Stability of Thin Reinforced Concrete Walls under Cyclic Loads: State-of-the-Art and New Experimental Findings

Angelica Rosso[1], João P. Almeida[2], Katrin Beyer[3]

Abstract

Damage to structural walls in the recent earthquakes in Chile (2010) and New Zealand (2011) demonstrated that modern reinforced concrete (RC) walls may not achieve the expected ductile response but could possibly be triggered by out-of-plane displacements of the wall. Following a review of the mechanisms that cause global out-of-plane buckling of RC walls, relevant international code requirements, and past experimental tests, this paper describes the findings from quasi-static cyclic tests of two thin RC walls with single layers of vertical and horizontal reinforcement. The two walls were subjected to uni-directional (in-plane) and bi-directional (in-plane and out-of-plane) loading respectively. Both walls experienced significant out-of-plane displacements and damage caused by out-of-plane deformations ultimately triggered the wall in-plane failure. The data obtained with extensive instrumentation of the test units, which included optical measurements of the 3D displacement field, yield new insights into the development of out-of-plane displacements, in particular with regard to: evolution of out-of-plane displacements with imposed in-plane displacements, portion of height and length of the wall that are involved in the out-of-plane instability, influence of both local and global tensile strains on the buckling behaviour and role of bi-directional loading on out-of-plane instability. The tests showed that very significant out-of-plane displacements—larger than half of the wall thickness—can take place without causing out-of-plane wall failure. The damage caused by these large out-of-plane displacements, however, can lead to a premature in-plane failure of the wall.

Keywords: Reinforced Concrete Walls, Thin Walls, Out-of-plane Instability, Large-scale Tests.

[1] Earthquake Engineering and Structural Dynamics Laboratory (EESD), School of Architecture, Civil and Environmental Engineering (ENAC), École Polytechnique Fédérale de Lausanne (EPFL), Switzerland.
EPFL ENAC IIC EESD, GC B2 495, Station 18, CH – 1015 Lausanne

angelica.rosso@epfl.ch

[2] Earthquake Engineering and Structural Dynamics Laboratory (EESD), School of Architecture, Civil and Environmental Engineering (ENAC), École Polytechnique Fédérale de Lausanne (EPFL), Switzerland.
EPFL ENAC IIC EESD, GC B2 484, Station 18, CH – 1015 Lausanne

joao.almeida@epfl.ch

[3] Earthquake Engineering and Structural Dynamics Laboratory (EESD), School of Architecture, Civil and Environmental Engineering (ENAC), École Polytechnique Fédérale de Lausanne (EPFL), Switzerland.
EPFL ENAC IIC EESD, GC B2 504, Station 18, CH – 1015 Lausanne

katrin.beyer@epfl.ch

1   Introduction

Recent earthquakes in Chile (2010, M_w 8.8) and New Zealand (2011, M_w 7.2) have shown that, despite many years of extensive research and subsequent design code advancements, several modern RC walls underperformed during these seismic events: even where ductile design details were adopted, the expected displacement capacities were not reached and new failure modes were observed (Elwood 2013; NIST 2014; Parra and Moehle 2014). Many of the observed walls in their failed configuration depict large out-of-plane displacements, see Fig. 1. This manuscript analyses the influence of global out-of-plane instability on the in-plane force-displacement response of walls.

At the outset, it is important to distinguish between global and local stability issues in the context of inelastic lateral response of RC walls. A global stability problem is considered to occur when a wall, subjected to in-plane loading, exhibits out-of-plane displacements (along a height similar or larger than the plastic hinge length) that lead to wall failure. On the other hand, local stability problems are mainly related to the buckling of longitudinal reinforcement bars over one or several tie spacings (Paulay and Priestley 1992). Local and global instability can influence each other mutually: (i) buckling of longitudinal reinforcement bars might be initiated by out-of-plane bending of the wall, which leads to unequal strain demands on bars in walls with two layers of reinforcement (NIST 2014); (ii) asymmetric rebar buckling in the wall thickness (as well as any other effect causing an asymmetric variation of stiffness at the local level, e.g. unequal concrete crushing, crack opening or compressive rebar yielding) may also increase the vulnerability of the wall to global buckling.

It is not always straightforward to identify, in post-earthquake reconnaissance missions, the extent to which a global instability phenomenon governed or at least influenced the behaviour and/or failure of collapsed walls: when residual relative out-of-plane displacements between the top and the bottom of the wall are present, this could indicate that an instability phenomenon took place, or that an in-plane failure of walls orthogonal to the wall under investigation occurred. On the other hand, a collapsed wall configuration like Fig. 1, where the top and bottom sections of the structural member are approximately aligned, suggests that buckling might have influenced the observed failure mode.

The impossibility of knowing the actual dynamic load time-history imposed to the members depicted in Fig. 1 (or in general to any member of real damaged structures) leaves necessarily some room for subjective interpretation regarding the experienced deformations that led to failure. Experimental tests, on the other hand, offer the possibility to observe the evolution of deformations. In the current manuscript the authors will present results of two tests on walls where the in-plane failure was triggered by out-of-plane deformations. These tests set themselves apart from others published in the literature (Section 4) as they are the first tests on walls that developed this failure mechanism for which the complete displacement fields of the walls were measured. This data allows new insights into the development of the out-of-plane failure mechanism.

Fig. 1 Example of out-of-plane induced damage in a RC wall after the New Zealand earthquake (Sritharan et al. 2014).

The out-of-plane instability treated in this paper is observed for walls that undergo large inelastic deformations (Goodsir (1985), Paulay and Priestley (1993) and Chai and Elayer (1999)). Member buckling is classically analysed in the context of theory of elastic stability (Timoshenko and Gere 1961). It will be seen later that global out-of-plane buckling of RC walls can also be considered as a geometrically nonlinear elastic response at the global level, despite being triggered by local inelastic phenomena, like crack opening-closing and compressive yielding of longitudinal rebars associated to cyclic loading. The latter phenomena will be reviewed in detail in the following section, which also recalls that the lateral stability of thin RC walls subjected to in-plane loading has been mainly investigated in the past by idealizing the end region of the wall (i.e., the vertical stripe near the wall lateral edge) as an axially loaded pinned-pinned (or simply supported) column. Therefore, available phenomenological models for predicting the out-of-plane failure have been developed and calibrated against results from cyclic axial tests on RC columns. These engineering models are very appealing as they are based on clear mechanics and have shown to yield conservative results, appropriate for design. However, since the boundary elements of the walls are simplified to an axially loaded column that is pinned at both ends, these models inevitably neglect certain parameters, such as the out-of-plane displacement profile along the wall length, the boundary conditions at the top, bottom and along the edge where the boundary element joins the web of the wall, and the effect of the in-plane moment gradient.

The objective of this paper is to contribute to the understanding of global out-of-plane failure modes of walls by analysing the response (namely the evolution of the monitored 3D displacement fields) from two walls that were recently tested at *École Polytechnique Fédérale de Lausanne* (*EPFL*), which were subjected to cyclic loading and where out-of-plane instability had a predominant role in the deformation mechanism and subsequent failure. The walls had T-shaped sections and single layers of vertical and horizontal reinforcement, and they were designed to be representative of the thin walls frequently used in current mid- and high-rise low-cost residential buildings in Colombia. The two walls were identical in terms of dimensions, reinforcement layout, applied axial load and shear span, but differed with regard to the applied displacement history: the first wall was subjected to in-plane displacements only, while the second was subjected to bi-directional loading (in-plane and out-of-plane displacements). The findings from these tests are compared to previous tests for which out-of-plane instability was observed and to the state-of-the-art models for the out-of-plane response of walls.

2   Description of Wall Instability and Existing Models

Pioneering works on out-of-plane stability of RC walls subjected to in-plane loading were published by Goodsir (1985), Paulay and Priestley (1993) and Chai and Elayer (1999). They describe the basic mechanics of wall buckling, identify some of the fundamental features triggering a potentially unstable out-of-plane response, and propose simple phenomenological models that can be applied in design. Very recently, following the observed out-of-plane failures in Chile and Christchurch, researchers have refocused their attention on this deformation mode, its effects on member failure (Sritharan et al. 2014), and advanced simulation techniques (Dashti et al. 2014a).

2.1   Mechanics of out-of-plane buckling

Paulay and Goodsir (Goodsir 1985; Paulay and Goodsir 1985) were the first to describe in detail the development of the out-of-plane failure mechanism for thin reinforced concrete walls, although such failure had been observed in earlier tests (Corley et al. 1981). For a wall with double layer reinforcement (Fig. 2), the mechanism can be summarised as follows: at large in-plane curvature demands the boundary element develops large tensile strains that cause wide near-horizontal cracks across the width of the wall and yielding of the longitudinal reinforcement in tension. Upon unloading, an elastic strain recovery takes place but due to the plastic tensile strains accumulated in the rebars, the cracks remain open. When reloading in compression and before crack closure, the compression force is resisted solely by the two layers of vertical reinforcement. This stage is typically accompanied by an incipient out-of-plane displacement, which occurs due to construction misalignments in the position of the longitudinal reinforcements or eccentricity of the resultant force C acting in this region, see Fig. 2(b). As long as the rebars retain their significant axial stiffness before yielding in compression, the out-of-plane displacements tend to remain small. However, as compression increases, the longitudinal rebar near the concave side (intrados of the out-of-plane deformed profile) yields, which leads to an abrupt reduction in out-of-plane stiffness and a consequent increase in the corresponding displacements. At this point, the second layer of longitudinal reinforcement—which has not yet yielded in compression—is the main source of out-of-plane

stiffness (Paulay and Priestley 1993). For RC walls with a single layer of reinforcement such a restraint does not exist leading hence to a much lower out-of-plane stiffness and larger out-of-plane displacements.

Depending on the magnitude of the tensile strain previously attained (i.e., before unloading), different scenarios can then take place as compression progresses (Paulay and Priestley, 1993): the cracks may close, re-establishing compressive force transfer through concrete and contributing to straighten up the wall, or they may remain open leading to compression yielding of the second layer of reinforcement. In the latter case, out-of-plane displacements will abruptly increase, possibly leading to wall buckling failure. Intermediate conditions, wherein the second layer of reinforcement yields but cracks still close, at least partially, are also conceivable. Independently of the scenario that effectively takes place, the occurrence of out-of-plane displacements and second-order moments will affect the in-plane wall response and should therefore be taken into account.

Following the previous rationale, the potential for out-of-plane buckling of walls has been shown to depend foremost on the maximum inelastic tensile strain in the vertical wall edge regions (Paulay and Priestley, 1993; Chai and Elayer, 1999), which has been since adopted as engineering demand parameter describing the likelihood of onset of lateral wall instability.
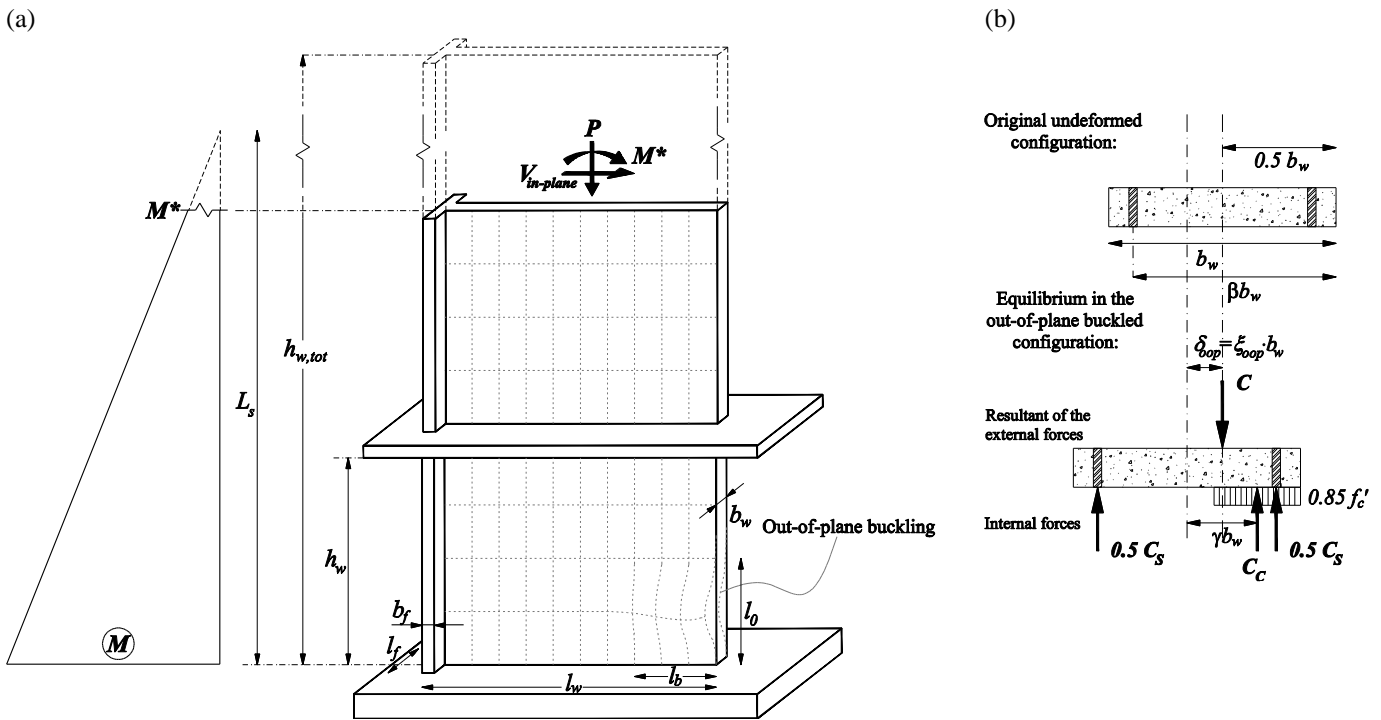
(a)   (b)

Fig. 2 a Wall geometrical characterization; **b** Equilibrium of external and internal forces at mid-height of buckling region, adapted from Paulay and Priestley (1993).

2.2   Brief review of existing models

This section briefly recalls and discusses some common assumptions of the two existing phenomenological models for the lateral stability of walls, which have been developed by Paulay and Priestley (1993) and by Chai and Elayer (1999). The model by Paulay and Priestley (1993) is applicable to walls with one or two longitudinal reinforcement layers, while the model by Chai and Elayer (1999) is applicable only to walls with two longitudinal reinforcement layers. It is therefore not suitable for the wall tests presented later in this paper but nevertheless it will be briefly discussed herein. These two models are based on axially loaded columns pinned at the extremities. These columns were used as proxy for boundary elements in plastic hinge regions of the wall. Under seismic loading, these regions are subjected to large amplitude tension and compression strains and are therefore the most susceptible to out-of-plane buckling. The idealization of the wall boundary elements over the plastic hinge region by columns requires some assumptions, which—in light of the tests on walls failing due to out-of-plane instability—might need to be revisited: (i) there are few indications on how to estimate or define the wall region that undergoes out-of-plane buckling—represented in Fig. 2(a) by $l_b \times l_0$—and how the latter relates to the longitudinal reinforcement layout, in particular the presence

of confined boundary elements; (ii) the influence of boundary conditions (both at the bottom and top of the column and along the edge that joins boundary element and web) and the strain gradient throughout the cross-section and along the wall height are lacking research; (iii) further, the validation of expressions to compute the buckling length l_0 need to be validated, which Paulay and Priestley (1993) and Chai and Elayer (1999) estimate as the plastic hinge length. The column idealization affects both models and the design of structures and experimental tests, which is discussed further in following sections.

In order to derive a stability criterion for walls, Paulay and Priestley (1993) formulated equilibrium for the deformed wall: Fig. 2(b) depicts the internal forces at mid-height of the buckling length l_0 where the out-of-plane displacement $\delta_{oop}=\xi_{oop}b_w$ is larger; ξ_{oop} is the normalized out-of-plane displacement and b_w is the section thickness. The total compression force C is taken by both the steel compression force C_S and the concrete compression force C_C, whose resultant is at an eccentricity γb_w. Assuming an equivalent rectangular compression stress block for the concrete compression force and that steel has reached its yield strength, vertical force and moment equilibrium yield the following expression for the eccentricity of the concrete compression force (for the definition of γ see Fig. 2(b)) (Paulay and Priestley 1993):

$$\gamma = \frac{1}{2}\left[\left(\xi_{oop}+0.5\right)-\sqrt{\left(\xi_{oop}+0.5\right)^2-2\xi_{oop}\cdot(1+1.176m)}\right] \tag{1}$$

where $m=\rho_b f_y/f'_c$ is the mechanical reinforcement ratio of the lateral vertical wall strip of length l_b, (ρ_b is the reinforcement ratio in the wall strip, f_y is the yielding strength of the rebars, and f'_c is the compressive strength of the concrete). This equation has a real number as a solution only when the term inside the square root is non-negative, i.e. when the following condition is respected:

$$\xi_{oop} \leq \xi_{oop,c}=0.5\cdot\left(1+2.35m-\sqrt{5.53m^2+4.70m}\right) \tag{2}$$

The previous equation represents the stability criterion of RC walls as derived by Paulay and Priestley (1993). The upper limit $\xi_{oop,c}$ is defined as the critical normalized out-of-plane displacement that marks the onset of wall instability.

The increase in arc length due to wall out-of-plane displacement results from the axial elongation of the wall strip over the buckling length l_0. Based on this assumption, Paulay and Priestley (1993) and Chai and Elayer (1999) established the following two relationships between the maximum average axial tensile strain $\varepsilon_{sm,c}$ over l_0 and the normalized out-of-plane displacement $\xi_{oop,c}$:

$$\varepsilon_{sm,c}=8\beta\left(\frac{b_w}{l_0}\right)^2\xi_{oop,c} \tag{3}$$

$$\varepsilon_{sm,c}=\frac{\pi^2}{2}\left(\frac{b_w}{l_0}\right)^2\xi_{oop,c}+3\varepsilon_y \tag{4}$$

According to both studies, l_0 may be taken as the equivalent plastic hinge length as computed by $l_p=0.20\cdot l_w+0.044\cdot L_s$, where l_w and L_s are respectively the horizontal length of the section and the shear span of the cantilever wall, see Fig. 2(a). It is considered that the buckling length $l_0=l_p$ should not need to be taken greater than 80% of the clear unsupported height h_w of the wall. Paulay and Priestley (1993) derived eq. (3) from geometrical considerations, where the parameter β takes into account the position of the vertical reinforcement within the wall thickness, as depicted in Fig. 2(b); it can therefore be applied to walls with one or two layers of longitudinal reinforcement. Eq. (4), developed by Chai and Elayer (1999), is a phenomenological equation based on tests of axially loaded concrete columns reinforced with two layers of vertical bars under large strains amplitudes. Therein, ε_y is the yield strain of the longitudinal reinforcement. This approach does not address the reduced out-of-plane stability expected for walls with a single layer reinforcement layout. Both equations above predict the tensile strain after which out-of-plane failure is expected.

Simulating out-of-plane instability of RC walls through numerical models has been seldom attempted because of the challenges related to the nonlinear geometrical and material behaviour described above, as well as the lack of experimental data for comparison purposes. To the authors' knowledge, the only attempts to model the wall out-of-plane buckling with finite elements

are the recent studies by Dashti et al. (2014a; 2014b), wherein curved shell elements were used to simulate the wall behaviour. This numerical tool gave promising results in terms of modelling the evolution of out-of-plane response and induced failure.

3   Code Requirements

In order to prevent out-of-plane instability of RC walls when subjected to seismic loading, the majority of international codes impose limits on the height to thickness ratio of walls. Only the New Zealand code includes more advanced models that are based on the work by Goodsir, Paulay and Priestley presented in the previous section (Goodsir 1985; Paulay and Priestley 1992; Paulay and Priestley 1993).

3.1   Eurocode 8, ACI 318 and NSR-10

In the Eurocode 8 (CEN 2004) the only requirements addressed to avoid out-of-plane instability are thickness checks and no specific prescriptions are given for walls with a single layer of reinforcement. The thickness of the wall web should satisfy the condition $b_w \geq max\{150 \text{ mm}, h_w/20\}$, where h_w is the clear storey height, see Fig. 2(a). Additional requirements apply with respect to the confined parts of the wall section: the thickness of the boundary elements of the wall should satisfy $b_b \geq 200$ mm. If the length of the confined part l_c does not exceed $max\{2b_w, 0.2l_w\}$ its thickness should be $b_b \geq h_w/15$, otherwise $b_b \geq h_w/10$. This requirement on the wall thickness is derived from the prescriptions related to the length of the confined boundary element l_c, since this length in turn depends on the compressive strains expected at the end of the wall. Considering that l_c depends directly on the neutral axis depth, which in the code is defined as $x_u = (\nu + \omega_v) l_w b_w / b_o$ (where ν is the axial load ratio, ω_v is the mechanical reinforcement ratio in the web, and b_o is the thickness of the confined core, as defined in CEN, 2004b), it is longer in walls with larger x_u.

The minimum wall thickness as defined in Eurocode 8 is to some extent contradictory to findings from the mechanical models and experimental findings: firstly, if the axial load ratio ν increases, the neutral axis depth x_u becomes larger and so does the required minimum thickness; past experimental tests (see Section 4), however, showed that larger axial loads reduce the potential for global instability since the maximum tensile strain attained decreases. Secondly, the Eurocode 8 relates the minimum wall thickness to the reinforcement ratio in the web ω_v while according to the mechanical models by Paulay & Priestley (1993) and Chai & Elayer (1999) the out-of-plane instability is related to the reinforcement ratio in the boundary element ρ_b, as can be noted from equation (2) (Rosso et al. 2014).

The two units tested and analysed later in this paper were designed according to the current Colombian design code (NSR-10 2010), which is largely based on the ACI Code (ACI Committee 318, 2011). According to these norms, two design methods are allowed: (i) The wall can be designed as a compression member subjected to a combination of axial, flexural and shear actions. In this case no explicit prescriptions on the minimum wall thickness are required, but they are considered implicitly through a limit $h_w/b_w \leq 12$ (note that this condition is a simplified summary of the code provisions for walls with a rectangular section braced against sidesway) that decides whether a second order analysis has to be carried out to take into account slenderness effects; (ii) As an alternative, the wall can be designed according to an empirical method, and in this case the thickness should respect the limit $b_w \geq max\{min\{h_w/25, l_w/25\}, 100 \text{ mm}\}$, where h_w is the clear storey height and l_w is the length. Finally, if $b_w > 250$ mm or $V > 2l_w b_w \lambda \sqrt{f'_c}$ (where V is the design shear force and λ is a modification factor for lightweight aggregate concrete) the reinforcement should be placed in two vertical layers within the wall section.

3.2   New Zealand Standard

The New Zealand Standard (Standards New Zealand 2006) dedicates an entire chapter on out-of-plane instability of thin walls. A first section consists in stability analysis of elastic members, providing general principles and design requirements to prevent Euler and flexural torsional buckling for slender walls. The section states that the structural walls should have a thickness $b_w \geq 100$ mm and if the latter is larger than 200 mm the reinforcement should be placed in two layers.

The second section, which addresses the stability of walls under seismic loading and is largely based on the studies by Goodsir, Paulay and Priestley (Goodsir 1985; Paulay and Priestley 1992; Paulay and Priestley 1993), provides further requirements for the minimum wall thickness in order to reduce the potential for out-of-plane buckling. Solving eq. (3) for the wall thickness and assuming $\varepsilon_{sm,c} \approx 0.0024 \mu_\Phi$, Paulay and Priestley (1993) derived the following relation for the minimum wall thickness: $b_w \geq 0.017 \cdot l_p \sqrt{\mu_\Phi / (\beta \cdot \xi_{oop,c})}$. Rewriting this equation using the relationship for the curvature ductility μ_Φ assumed by Paulay and Priestley (1993), one obtains:

$$b_w \geq \frac{0.017 l_p \sqrt{\dfrac{\mu_\Delta - 1}{3 l_p / L_s (1 - l_p / 2 L_s)} + 1}}{\sqrt{\beta \cdot \xi_{oop,c}}} = \frac{0.017 h_w \sqrt{\dfrac{2 - 2\mu_\Delta - 6 l_p / L_s + 3 l_p^2 / L_s^2}{3 - 6 L_s / l_p}}}{\sqrt{\beta \cdot \xi_{oop,c}}} \tag{5}$$

where the plastic hinge length is assumed to be, as mentioned above, $l_p = 0.20 \cdot l_w + 0.044 \cdot L_s$, where l_w and L_s are respectively the wall length and the shear span of the cantilever wall; β takes into account the reinforcement layout and it is assumed $\beta=0.8$ for doubly reinforced walls or $\beta=0.5$ for singly reinforced walls; μ_Δ takes into account the ductility and $\xi_{oop,c}$ is the critical normalized out-of-plane displacement, defined in eq. (2).

The New Zealand Standard (Standards New Zealand 2006) introduces several simplifications that apply to buildings with more than two storeys. For walls with axial load ratios larger than $v \geq 0.05$ the thickness of the boundary region of the wall section—extending over the lesser of the plastic hinge length or the full height of the first storey—should be:

$$b_w \geq \frac{k_m \mu_\Delta (L_s + 2 l_w)}{1700 \beta \sqrt{\xi_{oop,c}}} = \frac{\mu_\Delta h_w (L_s + 2 l_w)}{1700 \beta l_p \sqrt{\xi_{oop,c}}} \tag{6}$$

where the normalized out-of-plane displacement is computed as:

$$\xi_{oop,c} = 0.3 - \frac{\rho_b f_y}{2.5 f_c'} > 0.1 \tag{7}$$

The parameter β is assumed as $\beta=1$ for doubly reinforced walls or $\beta=0.8$ for singly reinforced walls; μ_Δ is assumed as $\mu_\Delta=5$ for limited ductile plastic regions or $\mu_\Delta=7$ for ductile plastic regions. The ratio of clear storey height to plastic hinge length $k_m = h_w / l_p < 1$ takes into account that when the buckling length exceeds the clear height of the wall in the first storey h_w, it is assumed to be 80% of h_w to make equation (6) not overly severe, in accordance with the Paulay and Priestley (1993) model. The buckling length is assumed to be equal to the plastic hinge length defined as $l_p = 0.25 \cdot l_w + 0.055 \cdot L_s$; note that this equation differs from the one suggested by Paulay and Priestley (1993).

A comparison between equations (2) and (7) for estimating the normalized out-of-plane displacement triggering out-of-plane failure, showed that the Paulay and Priestley (1993) relation gives larger values than New Zealand Standard (Standards New Zealand 2006) one. As a result of this observation and the foregoing noted difference between the equations for the plastic hinge length, the New Zealand Standard provides minimum thickness values that are in general about 40% larger than those computed using the Paulay and Priestley (1993) model.

4   Review of Past Experimental Tests

The lateral stability of thin walls subjected to in-plane loading has been mainly investigated by idealizing the lateral end region of the wall as an axially loaded column, leading researchers to perform several tests on slender RC prism units. These experiments, in which the units were subjected to tension and compression cyclic loading, provided useful information on many parameters influencing the out-of-plane behaviour.

The first author to perform such experiments was Goodsir (1985) and the main contribution from his study was the observation that the potential for instability of RC members is directly related to the maximum tensile strain reached before subsequent compressive loading. This finding was confirmed by several other experimental programs (Chai and Elayer 1999; Creagh et al. 2010; Chrysanidis and Tegos 2012; Shea et al. 2013). In the campaign by Creagh et al. (2010) and Chrysanidis and Tegos (2012), the specimens were tested under a single cycle of loading, i.e. subjected to tension and then compressed until failure; the results showed a strong influence of the tensile strain that was imposed during the first semi-cycle of tensile loading on the failure mechanism and out-of-plane instability. The test campaigns by Chai and Elayer (1999) and Shea et al. (2013) documented, in addition to the relation between susceptibility to out-of-plane failure and the maximum tensile strain, the influence of the thickness of the specimens and of the width of the cracks.

These test programs underlined that out-of-plane instability of walls is a complicated phenomenon, which depends on many different mechanical parameters. The hypothesis to study out-of-plane behaviour of walls by considering just the boundary element idealized as an axially loaded column may be a good assumption to understand some aspects of the buckling phenomenon, but it neglects several features influencing the out-of-plane response that can only be reproduced experimentally by tests on RC walls, as the authors will show in the following (see Section 2.2).

Unfortunately, very few of the past wall tests addressed specifically the behaviour of thin walls prone to out-of-plane buckling. The quasi-static cyclic tests for which significant global out-of-plane deformations along the wall height were observed or measured are summarised in Table 1. This data collection confirms that out-of-plane instability affects in general thin walls, both with one or two layers of longitudinal reinforcement, for which the ratio of shear span to thickness is larger than $L_s/b_w \geq 25$. All the test units were subjected to low axial load ratios ($v \leq 0.08$) and reached the same order of magnitude of maximum tensile strains. The normalized out-of-plane displacement $\xi_{oop,max}$ listed in Table 1 is the maximum attained before the cycle that led to failure. It was found that the behaviour of these test units before failure had many common features but the failure itself developed in different ways. Although Goodsir (1985) and Johnson (2010) did not elaborate on it, they observed that the maximum out-of-plane displacement occurred at approximately 0% in-plane drift, a finding which was confirmed by the tests that will be described in Section 5.

The failure modes developed by the walls in Table 1 are rather complex, as they often involve global wall instability, local bar buckling and concrete crushing. Roughly, following the comments in the Introduction, the failure modes can be grouped as follows:

(i)   Occurrence of global out-of-plane deformation of the wall contributes to trigger concrete crushing and spalling (e.g., walls 2 and 3 by Goodsir 1985; wall TW2 by Thomsen and Wallace 1995) and possibly rebar buckling (e.g., walls TW1 and TW4 by Almeida et al. 2014).

(ii)   Local buckling of rebars or concrete crushing on the compressed side of the wall (along the thickness, due to in-plane moments) may cause a large out-of-plane global deformation, which is typically still evident after failure (walls RWN and RWC by Johnson, 2010).

Table 1 Review of experimental tests on thin walls tested under cyclic loading which showed out-of-plane instability.

Test Unit	Ref.	Geom.	Scale	Layers of reinf.	l_w (mm)	b_w (mm)	$h_{w,tot}$ (mm)	h_w (mm)	L_s (mm)	L_s/b_w (-)	v (-)	$\xi_{oop,max}$ (-)	ε_{max} (-)	Comments
R2	Oesterle et al. (1976)	Rectang.	2:3	2	1905	102	4572	4572	4572	44.8	0	0.747[a]	0.011[b]	Due to the large unsupported height, at 1.67% drift the boundary element was 6.4 mm out-of-plane (ξ_{oop}=0.063) at 1100 mm above the base. This displacement increased rapidly, attaining 76.2 mm (ξ_{oop}=0.747) at 2.22% drift. The test was then temporarily halted to add lateral bracing, after which it was resumed. At 2.27% drift the wall strength drop exceeded 20% (due to the influence of the out-of-plane displacements) and the loading was stopped.
Wall 2	Goodsir (1985)	Rectang.	1:3	2	1500	100	2400	1000	3000-4000[c]	30-40[c]	0.03[c]	0.115[d]	0.020[e]	The out-of-plane deformation occurred over the full height of the wall between the base block and the floor slab. During the test the maximum out-of-plane displacement that was recovered was around 11.5 mm (ξ_{oop}=0.115) recorded at 600 mm above the wall foundation. After failure the measured out-of-plane displacement was approximately 40 mm occurring at 400 mm above the base block. At the end of the test the zone of transverse deformation extended about 600 mm from the wall edge. Increments of out-of-plane displacement occurred every time lateral force was reduced to zero.
Wall 3	Goodsir (1985)	T-shaped	1:3	2	1300	100	2400	1000	2500-4000[c]	25-40[c]	0.02[c]	0.150[d]	(na)	During the test, the maximum out-of-plane displacement attained and then recovered was around 15 mm (ξ_{oop}=0.150) measured at 250 mm above the foundation. During the last cycle before failure, when the test unit was close to zero in-plane load, a recovery of the lateral displacement took place, before increasing further. After failure, 200 mm below the floor slab, the lateral displacement was around 19 mm.
TW2	Thomsen and Wallace (1995)	T-shaped	1:4	2	1118	102	3658	914[e]	3658	35.9	0.08	(na)	0.022[e,f]	During the last cycle, while loading to 3.00% drift, the wall showed large out-of-plane displacements and at approximately 0.75% drift the test was stopped, since any further in-plane displacement would have caused a collapse of the web boundary element. Due to extensive concrete crushing, it was possible to observe that the longitudinal reinforcement was not buckling locally between two adjacent hoops, instead it was buckling globally over a large number of hoop spacings.
RWN	Johnson (2010)	Rectang.	1:2	2	2286	152	6096	6096	6096	42.1	0	0.087[a,g]	(na)	At 2.00% drift the test unit developed global instability. The test was terminated at 2.50% drift because of interference between the loading channels and the bracing system. In this test unit the tensile strains measured were larger in comparison to the ones measured in wall RWC. Failure eventually occurred due to local reinforcement buckling. The maximum out-of-plane displacement attained (ξ_{oop}=0.087) was measured at 1778 mm above the foundation.
RWC	Johnson (2010)	Rectang.	1:2	2	2286	152	6096	6096	6096	42.1	0	0.020[a,h]	(na)	At 2.00% drift the test unit developed global instability. The test was continued for three cycles until 4.00% drift only in one direction, since it was observed that the wall showed a lateral-torsional instability when crossing 0% drift in the reverse direction. Failure eventually occurred due to local reinforcement buckling. The maximum out-of-plane displacement attained (ξ_{oop}=0.020) was measured at 1524 mm above the foundation.
RWS	Johnson (2010)	Rectang.	1:2	2	2286	152	6096	6096	6096	42.1	0	0.092[a,h]	(na)	The test unit developed a wider crack at the wall-foundation interface. Until 1.50% drift the wall showed global instability, but then concrete degradation in the bottom region of the wall caused buckling and fracture of several bars leading to a local failure. The maximum out-of-plane displacement attained (ξ_{oop}=0.092) was measured at 1524 mm above the foundation.
TW1	Almeida et al. (2014)	T-shaped	2:3	1	2700	80	2000	2000	10000	125	0.05	0.581[i]	0.013[i]	During the two cycles at -0.75% drift large out-of-plane displacements were detected (ξ_{oop}=0.191, ξ_{oop}=0.324). While attempting to reach -1% drift in the web direction, the maximum out-of-plane displacement was attained (ξ_{oop}=0.581) and, after out-of-plane displacement recovery, failure occurred at around -0.75% drift. The out-of-plane displacements were detected at around midheight, they were fully recovered at each cycle and the maxima were observed always at around 0% drift.
TW4[j]	Almeida et al. (2014)	T-shaped	2:3	1	2700	80	2000	2000	10000	125	0.05	0.182[i]	0.009[i]	After the first clover-leaf cycle at 0.5% drift, at 0% in-plane drift and 0% out-of-plane drift the first significant out-of-plane displacement was detected (ξ_{oop}=0.058). The same happened after the first clover-leaf cycle at 0.75% drift (ξ_{oop}=0.167). At the start of a second cycle at 0.75% drift, while loading in the web direction, after an increase of out-of-plane displacement (ξ_{oop}=0.182) immediately recovered, a sudden failure of the wall occurred.

Legend: l_w: length of the specimen (see Fig. 2); b_w: thickness of the specimen (see Fig. 2), it refers to the central zone of the wall (web); $h_{w,tot}$: total height of the specimen (see Fig. 2); h_w: unsupported height of the specimen, i.e., in-between lateral supports (see Fig. 2); L_s: shear span (see Fig. 2); $v=N/(f_c l_w b_w)$: axial load ratio, defined as the ratio between the axial load and concrete strength times the gross area of the specimen; $\xi_{oop,max}=\delta_{oop,max}/b_w$: maximum normalized out-of-plane displacement, defined as the ratio between the maximum out-of-plane displacement and the thickness of the wall (see discussion in the text); ε_{max}: maximum tensile strain attained before failure. (na): data not available.

[a]Due to the large height of the specimen and/or to the lack of lateral restrains, the out-of-plane displacement was not recovered. This mechanism is not considered representative of a failure that may occur in buildings, where slabs reduce the vulnerability of the wall to out-of-plane instability. [b]Measured through strain gauges. [c]Depending on the in-plane direction in which the wall was loaded. The main purpose of this axial loading history (applied eccentrically) was to enhance the instability of one side of the wall, which was subjected to larger tensile (lower axial load) and compressive (higher axial load) strains. The corresponding axial load ratios in compression were 0.15(wall 2) and 0.12 (wall 3). [d]Two LVDTs were placed 150 mm from the end of the wall on the buckling side at 300 mm and 600 mm above the foundation. [e]The slabs were not restrained. [f]After 1.50% drift the strain gauges stopped acquiring data. [g,h]String pots were connected to the wall, on both ends, at 5842 mm and 6096 mm [f], or 3099 mm, 5842 mm and 6096 mm [g] above the foundation; moreover, an optical measurement system was used. [i]Calculated through an optical measurement system. [j]Tested under bi-directional loading.

5 Findings from New Cyclic Tests on Thin RC Walls

5.1 Test setup, loading and instrumentation

Within an experimental program on RC walls carried out at *EPFL*, five test units at 2:3 scale were subjected to quasi-static cyclic loading. The first three walls (TW1 to TW3) were tested under in-plane loads, while the last two specimens (TW4 and TW5) were loaded under a combination of in-plane and out-of-plane loading. The walls TW1 and TW4, which were geometrically identical, had the smallest wall thickness and the largest shear span ratio (see description of the test setup below). Only these two walls developed significant out-of-plane displacements and will be discussed in the following. Their dimensions and reinforcement details, which follow current design practices for low- to mid-rise construction of residential buildings in Colombia, are shown in Fig. 3.

The two walls were 2000 mm tall, 80 mm thick and 2700 mm long. The walls had at their North end a flange that was 80 mm thick and 440 mm long. The short flange was included to study the effect of a perpendicular wall on member stability and damage distribution. In the following the South extremity of the wall is referred to as 'web edge'. According to the aforementioned detailing practice, the longitudinal reinforcement consisted of a single layer of reinforcement, with 11 rebars with diameter d_w=6 mm, 3 rebars with d_b=16 mm in each boundary element, and 4 rebars with d_w=6 mm in the flange; only the small diameter bars were spliced at the base of the wall (splice length of 350 mm). The transverse reinforcement consisted of bars with d_t=6 mm, spaced at 200 mm. Since the reinforcement was placed along a single layer, the bars were positioned with a slight eccentricity with respect to the centreline of the section. The vertical rebars were thus closer to the East side of the wall, as can be noted in Fig. 3 (section B-B). The foundation was 3600 mm long, 700 mm thick and 400 mm tall; it was designed as a rigid support for the wall and connected to the strong floor with six prestressed bars. During the tests the axial load ratio was maintained constant and equal to 5%.The main material properties of the test units were: f_y=460 MPa for the 6 mm bars, f_y=565 MPa (TW1) and f_y=515 MPa (TW4) for the 16 mm bars, and f'_c=28.8 MPa (TW1) and f'_c=31.2 MPa (TW4) for the concrete.
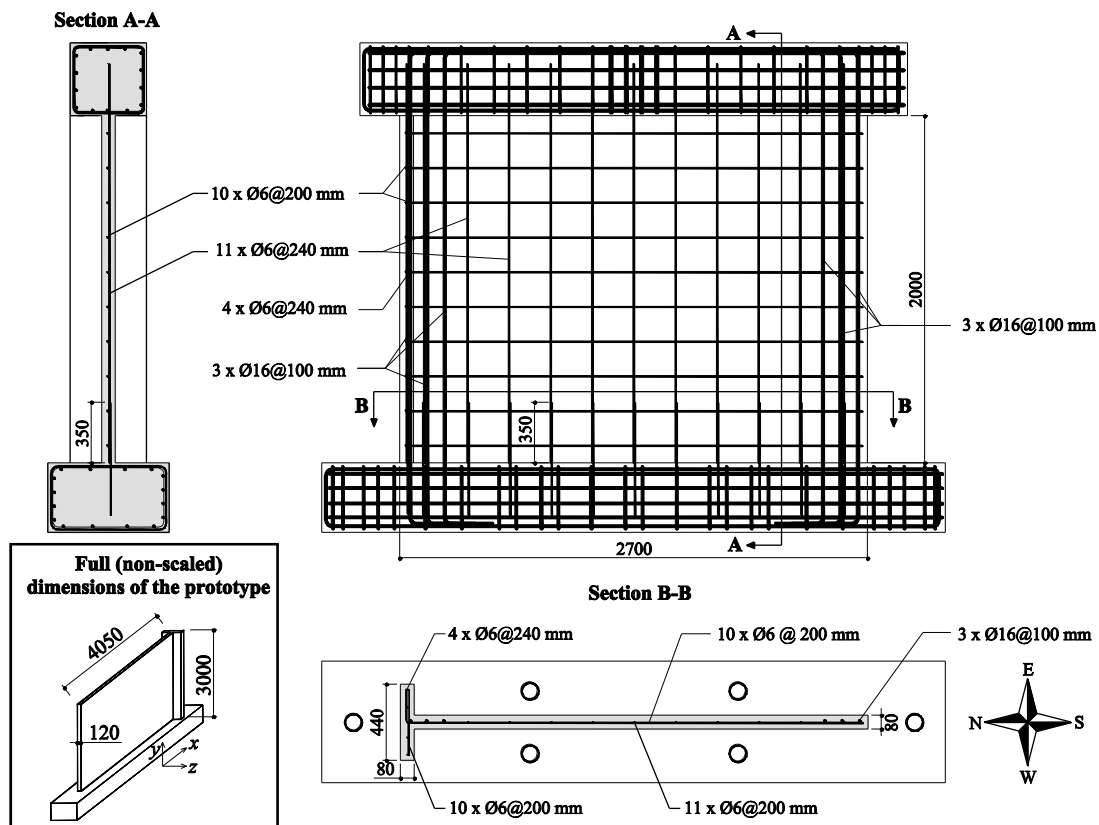
Fig. 3 Geometrical characterization and detailing of test units TW1 and TW4, constructed at scale 2:3, and dimensions of the corresponding wall at full-scale in the bottom left corner (in mm).

1 A sketch of the general test setup used in the experiments is shown in Fig. 4(a). A rigid steel beam was placed on the top of the
2 RC beam, to warrant a distributed application of the vertical loads. Two vertical actuators were connected to the steel beam close
3 to the wall ends to apply simultaneously the axial load acting on the wall and the bending moment required to achieve the desired
4 shear span of 10 m (corresponding to a shear span ratio of 3.7). The latter was achieved by coupling the control of these two
5 actuators to a third horizontal one, connected to the top RC beam to impose the in-plane loading (these three actuators are
6 represented in red in Fig. 4(a)). For the wall TW4, which was subjected to bi-directional loading, two additional horizontal
7 actuators were connected to the top RC beam to impose the out-of-plane displacements (green actuators in Fig. 4(a)).

8 For the wall test TW1, in order to prevent out-of-plane displacements at the storey height, four steel tubes—visible in Fig. 7(a)—
9 were placed at the height of the top RC beam. The axial forces in these tubes were derived from strain gage measurements. The
10 loading protocol consisted of a reversed quasi-static cyclic history, imposed by the horizontal actuator in displacement control.
11 Two fully-reversed cycles were applied at each target drift, according to the following incremental drifts: $\pm 0.05\% \rightarrow \pm 0.1\% \rightarrow$
12 $\pm 0.15\% \rightarrow \pm 0.25\% \rightarrow \pm 0.35\% \rightarrow \pm 0.5\% \rightarrow \pm 0.75\% \rightarrow \pm 1\%$. A full description of the corresponding load stages (LS) is
13 represented in Fig. 5(a) and Fig. 6(a).

14 Concerning the test unit TW4, the top RC beam was controlled in the out-of-plane direction by the actuators placed in this
15 direction. The loading protocol consisted of a quasi-static cyclic history following a 'clover leaf' pattern, which was imposed by
16 the horizontal in-plane and out-of-plane actuators in displacement control. One clover leaf cycle was applied at each target drift;
17 at large values of drift, clover leaf cycles were also applied in the opposite sense. The following incremental history was
18 followed for the in-plane and the out-of-plane directions, respectively: $\mp 0.05\% \rightarrow \mp 0.1\% \rightarrow \mp 0.15\% \rightarrow \mp 0.25\% \rightarrow \mp 0.35\% \rightarrow$
19 $\mp 0.5\% \rightarrow \mp 0.75\%$ and $\mp 0.05\% \rightarrow \mp 0.1\% \rightarrow \mp 0.15\% \rightarrow \mp 0.25\% \rightarrow \mp 0.35\% \rightarrow \mp 0.5\% \rightarrow \pm 0.5\% \rightarrow \mp 0.75\% \rightarrow \pm 0.75\%$. Fig.
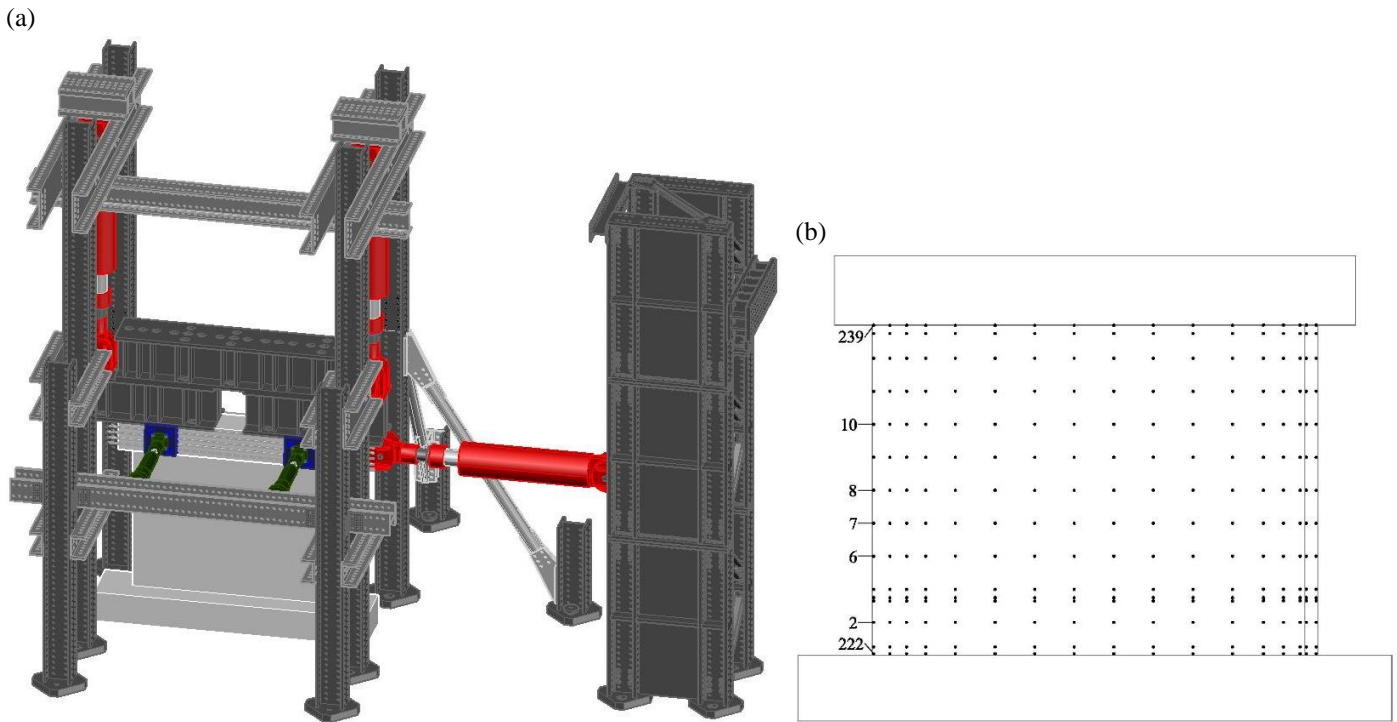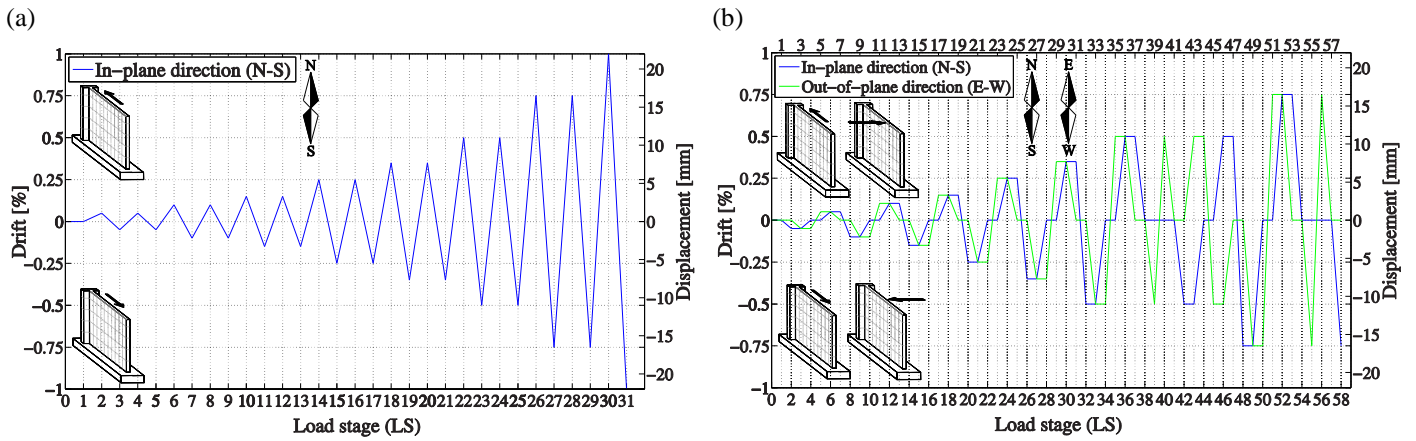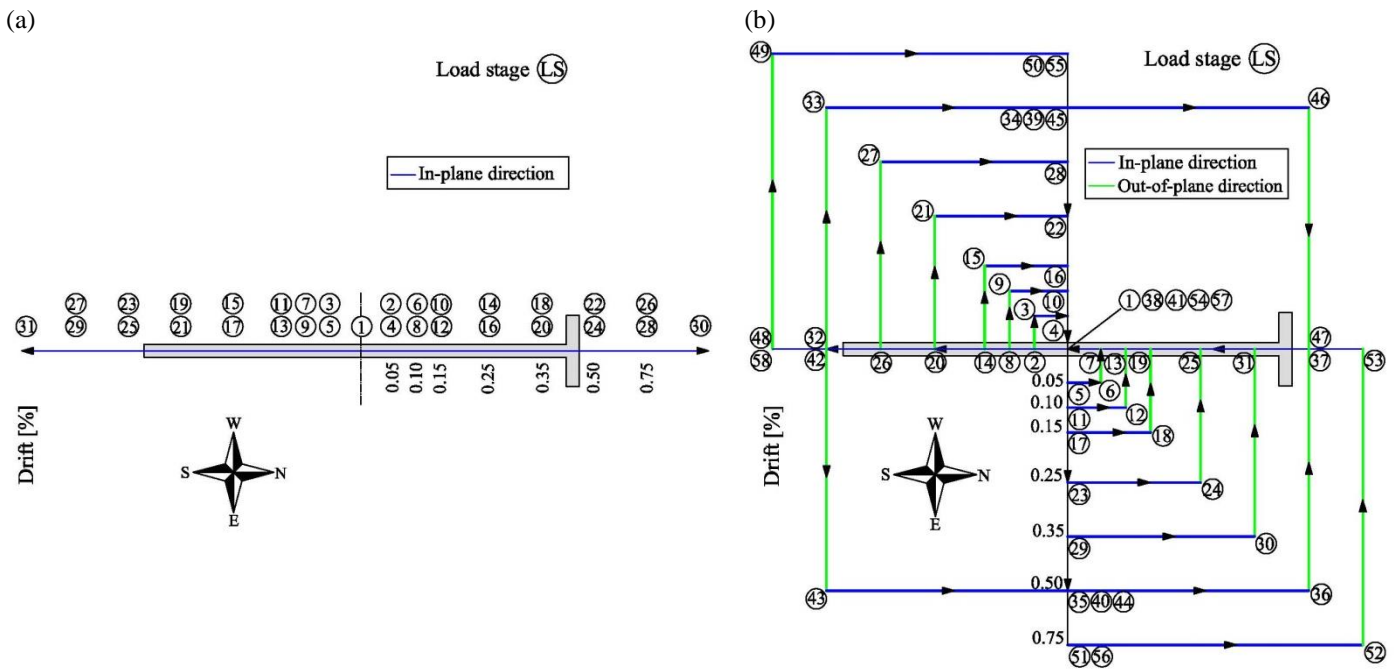20 5(b) and Fig. 6(b) describe the corresponding load stages.

(a)

(b)

21 **Fig. 4 a** 3D representation of the test setup; **b** LED grid used for the optical measurement system (with identification of LEDs
22 no. 6, no. 7, no. 8, no. 10 no. 222, and no. 239 at the wall web edge).

23

(a)

(b)

Fig. 5 Drift protocols of the two quasi-static cyclic tests, including load stages (LS): **a** wall TW1; **b** wall TW4.

(a)

(b)

Fig. 6 In-plane representation of the two loading protocols, including load stages (LS): **a** wall TW1; **b** wall TW4.

The walls were instrumented using conventional and optical measurement systems. Load cells in the actuators recorded the applied forces. The in-plane and out-of-plane deformations of the wall surface were measured using a grid of 255 LEDs on the East face of the wall (Fig. 4(b)), whose 3D coordinates were recorded with the optical measurement system NDI Optotrak Certus HD (NDI 2009). LVDT and DIC measurements completed the instrumentation system but are not used in the following. During the loading phases, videos were recorded and at each load stage photos were taken and progression of cracking was traced. A more detailed account of the experimental setup, test results and material properties can be found in Almeida et al. (2015).

In order to set the test units, which were constructed at 2:3 scale, into context with current construction practice, the corresponding prototype wall dimensions were compared against the limits included in building codes (Section 3). The full (non-scaled) web width of the prototype wall is 120 mm and has also a single layer of longitudinal reinforcement. The results for the different codes are summarized in Table 2. The table shows that the reinforcement layout with one longitudinal reinforcement layer complied with requirements in all codes (EC8 does not give any specifications for walls with single layer reinforcement). It also underlines that the limits on wall thickness that are included in ACI-318 and NSR-10, which the wall meets, are much less stringent that those in EC8 and NZS-3101, which would not allow the proposed design.

Table 2 Checks on dimension limits for walls TW1 and TW4 according to some international codes. All dimensions in millimeters.

	EC8		NZS-3101		ACI-318 / NSR-10	
	Limit	Check	Limit	Check	Limit	Check
Thickness of the boundary element (b_w=120 mm)	≥200	✗	≥179[a]	✗	≥100	✓
Thickness of the web (b_{w0}=120 mm)	≥150	✗	≥100	✓	(-)	(-)
Single reinforcement layer allowed	(-)	(-)	<200	✓	<250	✓
[a]The displacement ductility has been assumed as μ_Δ=5. (-) Not addressed by the code.						

5.2 Description of the experimental behaviour of both test units

This section presents a short qualitative description of the behaviour of the test units. In wall TW1, cracks started forming since the first cycles. They were mainly horizontal, confirming the flexural behaviour expected from the imposed large shear span ratio. During loading LS26→LS27 (in-plane drift amplitude: δ_{ip}=±0.75%), the wall began to show evident out-of-plane displacement towards West, but the latter was recovered completely before reaching LS27. The same response, with larger out-of-plane displacements attained, was observed when loading LS28→LS29 (δ_{ip}=±0.75%). Finally, during loading LS30→LS31 (δ_{ip}=±1%) and following the large out-of-plane deformations visible in Fig. 7(a) and the progression of concrete crushing, a local buckling of the longitudinal rebars in the bottom part of the boundary element at the free web edge took place. As depicted in Fig. 7(b), after failure the overall out-of-plane displacements were not apparent. Post-failure observations indicate that the reinforcing bars buckled in the opposite direction to the global out-of-plane deformations, and the rebar d_b=16 mm closer to the web edge buckled more than the second, and this one more than the third rebar in the boundary element, see Fig. 7(b).

Wall TW4 also showed a flexural behaviour from the first load stages, with the appearance of mainly horizontal cracks. At LS36 (δ_{ip}=0.5%) crushing of the concrete was first observed, occurring at the wall base of the web end. At LS48 (δ_{ip}=-0.75%) first spalling of the concrete took place and from LS54 (δ_{ip}=0%) an out-of-plane deformed shape towards West could be observed even with the naked eye. During loading LS57→LS58 (δ_{ip}=±0.75%), following progression of concrete crushing and spalling of cover concrete, partially promoted by rebar buckling, a sudden failure took place. After an increase of the overall out-of-plane displacement, then completely recovered, the failure involved abrupt concrete crushing and buckling of the rebars in the boundary element at the free web edge. Post-failure observations indicate that the reinforcing bar d_b=16 mm closest to the wall end buckled in the opposite direction to the global out-of-plane deformation, while the second rebar buckled in the same direction, see Fig. 7(c). Concerning the overall out-of-plane displacements, while in TW1 the maximum was observed always in-between load stages and the wall straightened before the end of each such cycle, in TW4 this trend was less clear and in several load stages—in which the web was in compression—the out-of-plane deformation remained evident.

Along the same rationale of using the concept of an equivalent column to describe the wall web edge behaviour, and considering the actual boundary conditions of the test unit, one could think to the simplified beam model depicted in Fig. 8. Therein, the top rotational spring simulates the torsional stiffness of the top RC wall and slab, while the distributed axial load (assimilated to a constant load) represents the change in the axial force of the web edge modelled as a column. In a wall this change results from the moment gradient and diagonal compression from shear forces. Finally, a fixed bottom end is assumed to be representative of the effective boundary condition at the base of the test specimen. This model is currently being developed and validated by the authors to carry out finite element simulations that can be employed in engineering practice to assess the out-of-plane instability of wall boundary elements.

The direction in which the wall experienced out-of-plane instability was the same for both test units. The out-of-plane global displacement occurred towards West, so that the concave side of the wall (intrados of the out-of-plane deformed profile) corresponds to the face on which the LEDs were placed, as shown in Fig. 7(a) for TW1. Bearing in mind the beam model described above, this occurrence can be explained by the fact that the single layer of longitudinal reinforcement is placed with a slight eccentricity to the centreline of the wall section, see Fig. 3; therefore, when the cracks are still open and the compression force is resisted solely by the steel bars, an out-of-plane moment develops inducing the wall to buckle towards the opposite side where the reinforcement is placed, see Fig. 8(b).

13

1 As outlined before, in both test units the buckling of the outermost rebar above the foundation occurred in the opposite direction
2 to the global wall out-of-plane deformation. Again referring to the simplified beam model of Fig. 8, such phenomenon can be
3 ascribed to the fact that, due to the fixed support at the base of the wall, the moment at the base is in the opposite direction than
4 the moment at midheight..

(a) (b) (c)
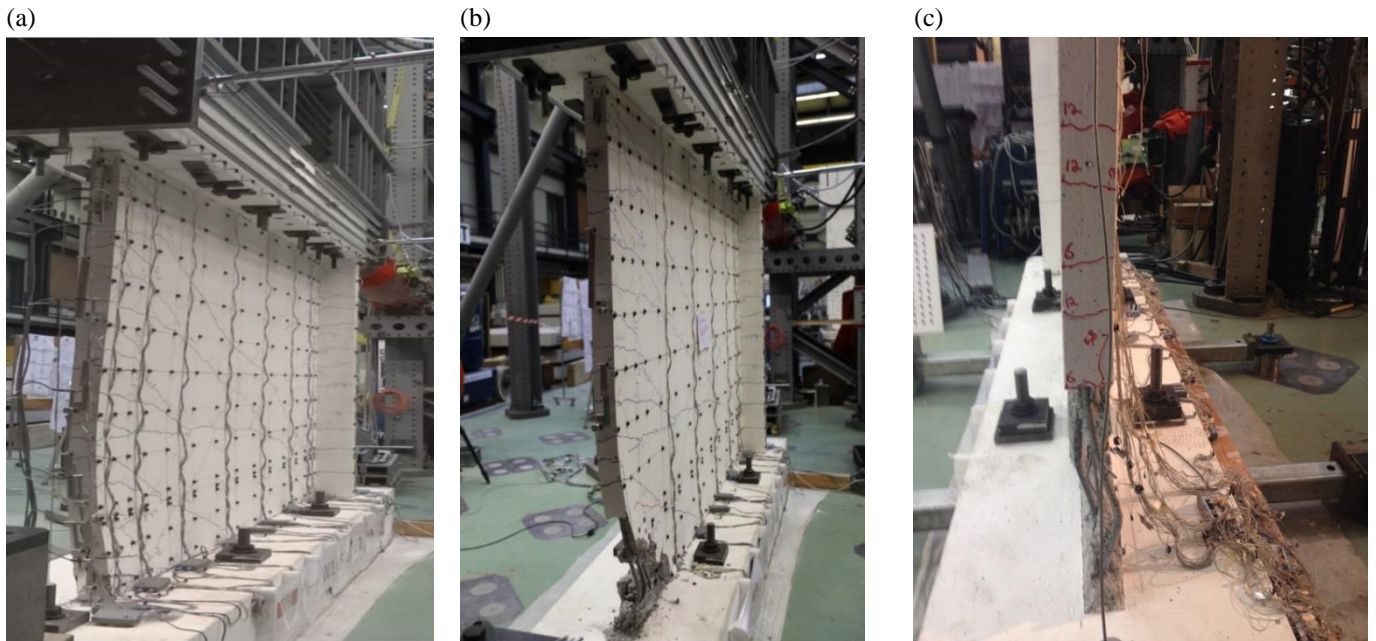
5 **Fig. 7 a** Deformed shape of wall TW1 at loading LS30→LS31, around 0% in-plane drift; **b** wall TW1 at the end of the test, after
6 failure; **c** wall TW4 at the end of the test, after failure.

(a) (b)
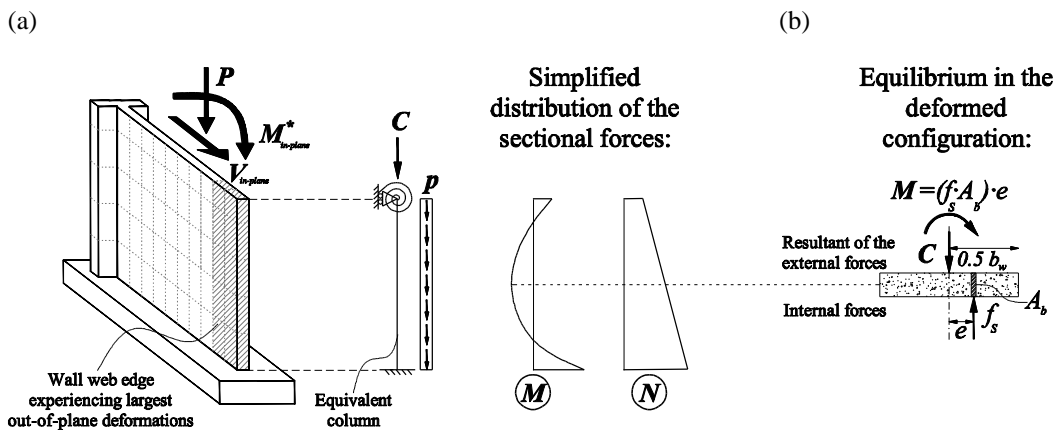
7 **Fig. 8 a** Equivalent beam model for wall web edge with corresponding loads. **b** Equilibrium of external and internal forces in a
8 section where the crack crosses the entire thickness.

9 Fig. 9(a) describes the in-plane force-displacement responses of wall TW1, wherein a stable hysteretic behaviour with
10 appreciable dissipation of energy can be observed. The plot includes indications of all load stages after LS26, which corresponds
11 to the critical phase of the structural behaviour. Focusing on the last loading cycle, between LS30 and LS31 ($\delta_{ip}=\pm1\%$), Fig. 9(a)
12 reflects the cyclic stiffness and strength degradation that took place upon approaching the peak drift of the previous cycle ($\delta_{ip}=-$
13 0.75%), at which a drop of approximately 30% of the force capacity can be observed. The wall failed soon after due to crushing
14 and rebar buckling, and the strength dropped quickly to zero. It is noted that the stiffness degradation that occurred during
15 LS30→LS31 initiated when returning from positive drifts and approaching 0% in-plane drift (marked with a circle), which
16 unmistakably puts into evidence the role of the large out-of-plane deformations in the deterioration of the wall in-plane resisting
17 mechanism. The point at which strength degradation starts is also identified with a circle in Fig. 10(a), showing the out-of-plane
18 displacement *versus* the wall in-plane displacement, which will be discussed later in detail.

14

1　The observed failure mode was an in-plane failure which had been triggered by damage induced by out-of-plane deformations.
2　Until the last cycle it seems that the out-of-plane displacements were largely elastic deformations, while in cycle LS30→LS31, at
3　the maximum out-of-plane displacement, permanent inelastic deformations—due to concrete crushing and possibly compressive
4　steel yielding—occurred. Due to these inelastic deformations, the out-of-plane displacements could not be fully recovered (see
5　the residual normalized out-of-plane displacement of around 0.08 in Fig. 10(a)) and the damage caused a stiffness degradation,
6　which then lead to an in-plane premature failure. In other words, although the collapse occurred at a local level, it was mainly
7　triggered by the development of a global mode of deformation.

(a)　　　　　　　　　　　　　　　　　　　　　　　　　　(b)
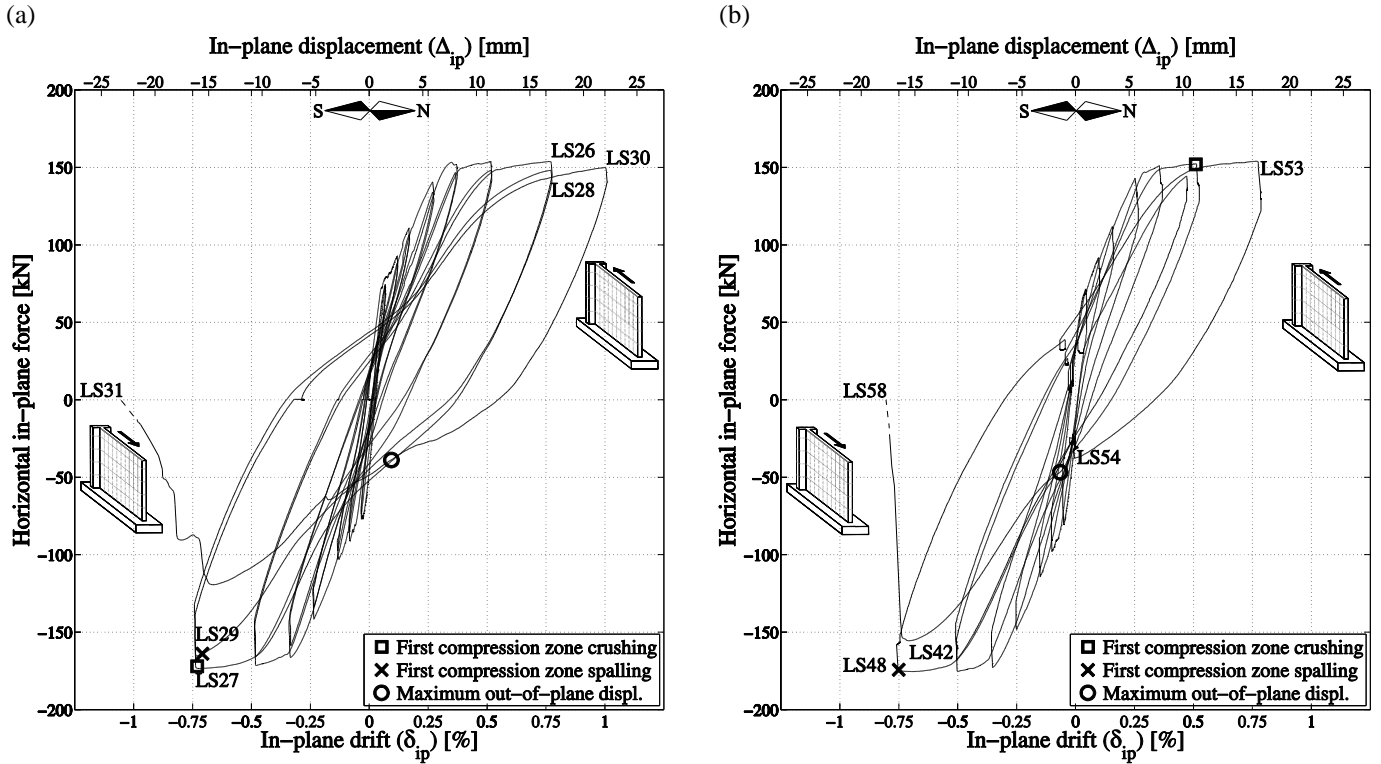
8　**Fig. 9** In-plane force-displacement response: **a** wall TW1; **b** wall TW4.

(a)　　　　　　　　　　　　　　　　　　　　　　　　　　(b)
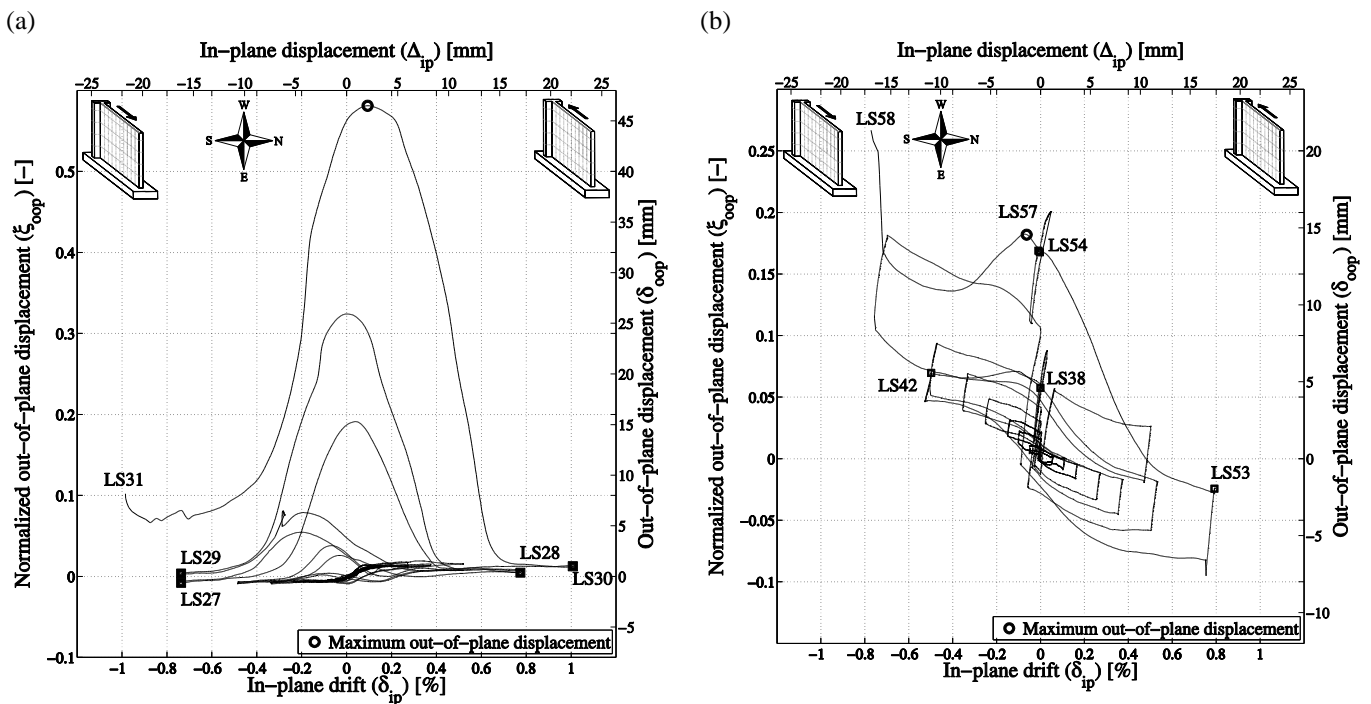
9　**Fig. 10** Imposed in-plane drift *vs* normalized web edge out-of-plane displacement at the height where maximum out-of-plane
10　displacement was measured, i.e. at marker no. 7 in Fig. 4(b): **a** wall TW1; **b** wall TW4.

A similar behaviour was observed for wall TW4, see Fig. 9(b): when loading from the flange to the web edge, during the last cycles the wall showed clear signs of cyclic stiffness and strength degradation. Focusing on the final cycle LS57→LS58 ($\delta_{ip}=\pm0.75\%$), the in-plane capacity of the wall dropped suddenly upon reaching -0.70% in-plane drift and, similarly to TW1,, the more evident stiffness degradation initiated at the in-plane drift (marked with a circle in Fig. 9(b)) for which the maximum out-of-plane deformations were reached (circle in Fig. 10(b)).

From Fig. 10(b) it can be also noted that in cycle LS53→LS54 (from 0.75% to 0% in-plane drift, maintaining 0% out-of-plane drift) while unloading the out-of-plane displacements increased considerably. They augmented even further while loading beyond LS57 (from 0% to -0.75% in-plane drift, maintaining 0% out-of-plane drift). This observation confirms the tendency previously discussed for wall TW1, that at around 0% in-plane drift the out-of-plane deformations were close to the maxima attained during the load history.

5.3   Analysis of global-level response quantities

The aim of this section is to compare the hypotheses and estimates of the existing models to predict the out-of-plane behaviour with the results obtained from the experimental tests described in the previous sections. Reasons for the observed discrepancies are identified and new estimates of fundamental parameters related with stability of walls are provided. They will be used in future research for the development of new models and methods of simulation.

5.3.1   *Normalized out-of-plane displacements*

Paulay and Priestley (1993) postulated that an upper bound out-of-plane displacement that triggers failure by out-of-plane buckling corresponds to half the wall thickness b_w, i.e., when $\xi_{oop}=0.5$, see Fig. 2(b). They also assumed that, in a real structure, failure should occur at a smaller eccentricity and hence from the equilibrium considerations and assuming a limited compressive strength of the concrete the stability criterion of eq. (2) was derived (Section 2.1). Later, the same criterion was used by Chai and Elayer (1999).

Referring to Section 4, it is interesting to observe that the only test units where maximum out-of-plane displacements larger than 0.5 times the wall thickness were recorded were TW1 (current work) and R2 (Oesterle et al. 1976). In the case of the wall R2, however, the boundary conditions do not reproduce those of a real building since the wall was not braced laterally at the height of the floor slabs. It is possible, that in other wall tests maximum out-of-plane displacements with $\xi_{oop}>0.5$ took also place but were not recorded. For most tests the out-of-plane displacement measurements were limited to single points (string pots at fixed heights) and it is therefore possible that the out-of-plane displacements might not have been measured where they were largest. For TW1, on the other hand, the dense grid of LEDs—shown in Fig. 4(b)—provided the complete displacement field over the wall height and along its length, thus ensured that the maximum out-of-plane displacement could be monitored. In TW1 a maximum normalized out-of-plane displacement above 0.5 was attained (more precisely $\xi_{oop,max}=0.581$ for LED no. 7, see Fig. 10(a)).

In Fig. 11 the horizontal axes represent the normalized out-of-plane displacements and the vertical axes show the mean axial strain as computed from the variation in length between the markers at the foundation and the top RC beam using the three spatial coordinates of the markers (LEDs no. 222 and no. 239, shown in Fig. 4 (b)). Note that the stability criterion by Paulay and Priestley (1993) yields a maximum out-of-plane displacement of $\xi_{oop,c}=0.123$ for TW1 and of $\xi_{oop,c}=0.136$ for TW4, which are rather conservative estimates of the actually attained out-of-plane displacements (Fig. 11 (a) and (b)). Wall TW4 attained smaller values of out-of-plane displacement in comparison with TW1, but the behaviour shown during the last cycle is quite similar: as evidenced in Fig. 10(b) the maximum out-of-plane displacement ($\xi_{oop,max}=0.182$ at LED no. 7) was attained around zero in-plane drift and then partially recovered before failure.

5.3.2   *Height of the wall involved in the out-of-plane behaviour*

One important input quantity for the assessment of the out-of-plane stability of walls is the height l_0 along which out-of-plane buckling develops. It has been suggested (Paulay & Priestley, 1993; Chai & Elayer, 1999) that l_0 can be taken as the equivalent plastic hinge length l_p since large strains may be expected only over the lower part of the wall,. Besides, l_0 should be less than 80% of the clear unsupported height of the wall, which is typically equal to the storey height h_w. For TW1 and TW4, the buckling

length as proposed by Paulay & Priestley (1993) yields $l_0=l_p=0.20l_w+0.044L_s=980$ mm, which corresponds to approximately half the storey height. From Fig. 12, however, it can be observed that out-of-plane deformations involve roughly the entire storey height, i.e., $l_0=h_w$. Expressions for wall plastic hinge lengths also seem to inadequately estimate the actual buckling length observed in other experimental tests (Goodsir 1985; Thomsen and Wallace 1995). Therefore, with a view to developing future models, the previous assumption of $l_0=l_p$ should be revised, as already pointed out by other authors (Johnson 2010). Based on the results of TW1 and TW4, the inflexion points can be identified and hence an arguably more reasonable estimate for the buckling height is roughly $0.75 \cdot h_w$.

(a) (b)
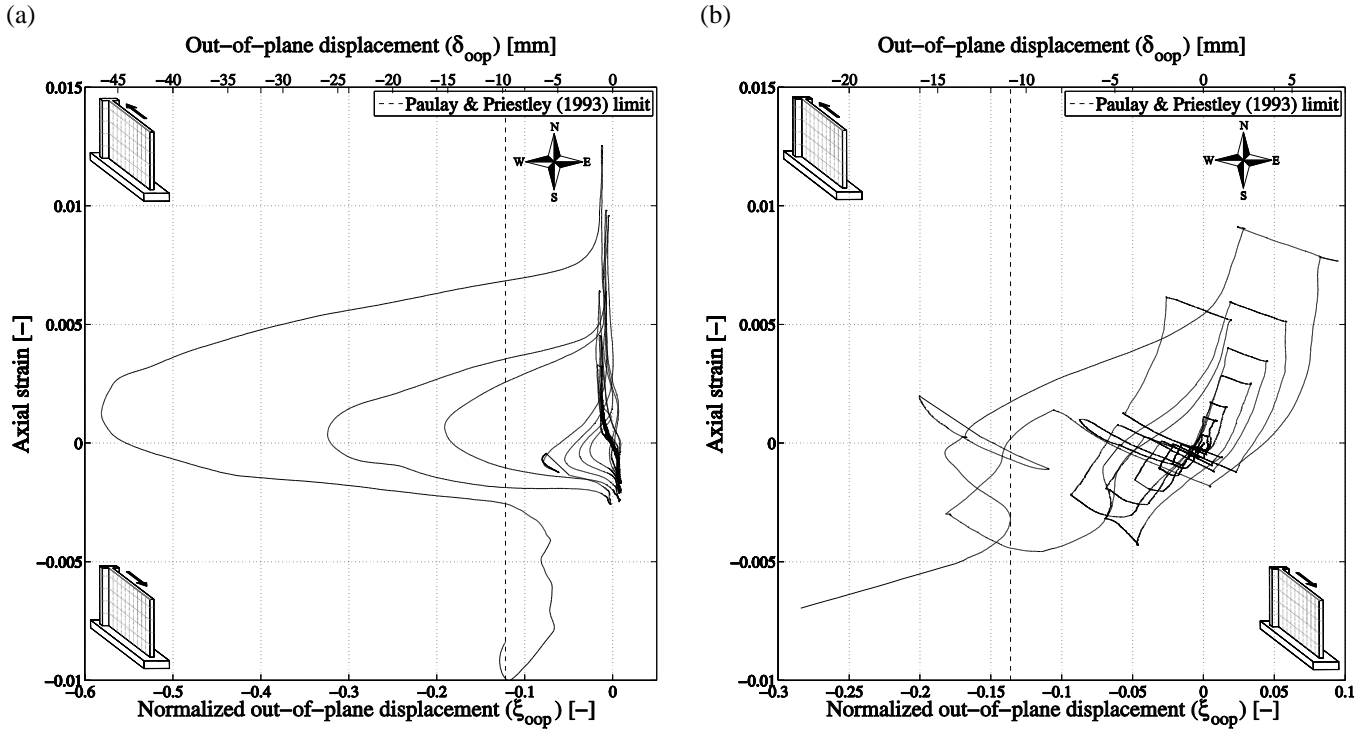
Fig. 11 Normalized out-of-plane displacement *vs* axial strain (computed between LEDs no. 222 and no. 239, see Fig. 4(b)): **a** wall TW1; **b** wall TW4.

(a) (b)
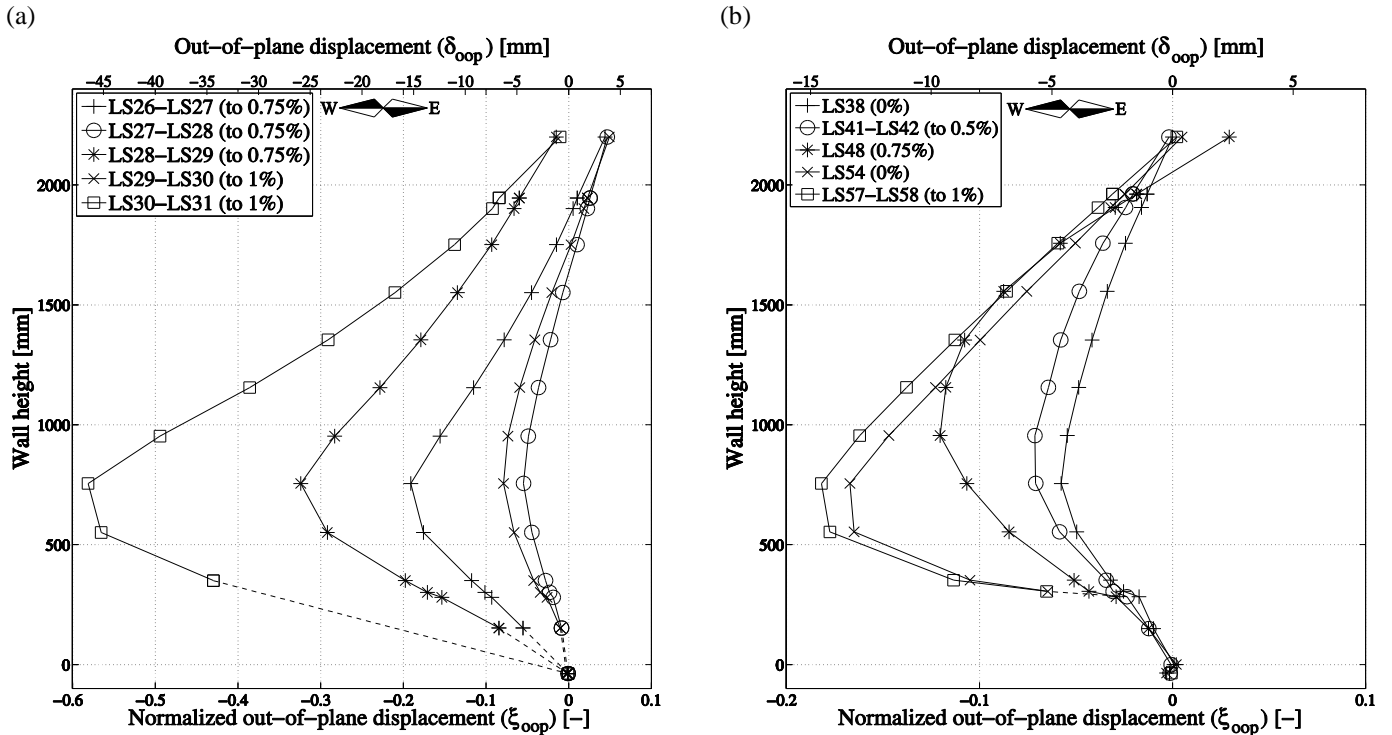
Fig. 12 Normalized web edge out-of-plane displacement profile along the wall height in-between or at specified load stages: **a** wall TW1; **b** wall TW4 (only profiles at which 0% out-of-plane drift was imposed are presented in this figure).

17

5.3.3   Length of the wall involved in the out-of-plane behaviour

2   Using the experimental results of TW1 and TW4 the distribution of the out-of-plane deformations along the wall length was
3   investigated: namely Fig. 13 plots the normalized out-of-plane displacements along the wall length at the height where the
4   maxima out-of-plane displacements were measured (i.e., 755 mm above the foundation). It is noted that the deformed shapes are
5   similar for both walls, putting into evidence the difficulty of identifying a region from the web edge in which the out-of-plane
6   deformations concentrate. Other researchers (Goodsir 1985) also reported that instability involved a quite significant length of
7   the wall. The significant restraining effect that the part of the wall going into tension exerts on the buckling region should hence
8   be taken into account in the development of appropriate simulation methods, namely those based on the use of an equivalent
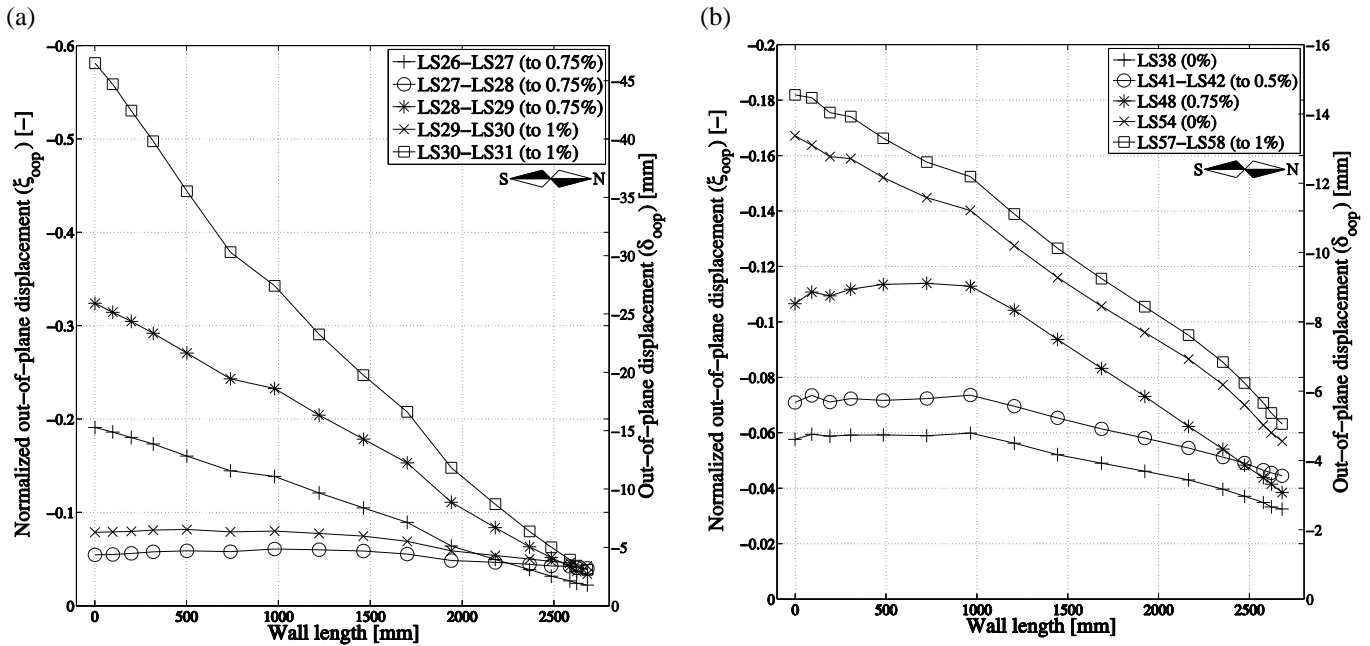9   idealized column under axial loading.

10 **Fig. 13 a** Maximum out-of-plane displacement profile along the wall length (at 755 mm above the foundation), in-between or at
11 specific load stages: **a** wall TW1; **b** wall TW4 (only LS at 0% out-of-plane drift are presented in this figure).

12

13 *5.3.4   Influence of the bi-directional loading on the out-of-plane behaviour*

14 As mentioned above, the only difference between the experimental tests of TW1 and TW4 was the application of out-of-plane
15 loads in the latter case. Wall TW4 failed at the beginning of the second clover leaf cycle at 0.75% drift, when loading from the
16 flange to the web edge—see Fig. 6(b)—at a smaller value of drift in comparison to TW1, which sustained a first cycle at 1% in-
17 plane drift in the flange direction. Even if this evidence is not surprising, a clear explanation on how the bi-directional loading
18 affected the development of a premature failure is not straightforward.

19 Fig. 14(a) presents a rectified normalized out-of-plane displacement profile along the wall height for TW4, at specific load stages
20 when out-of-plane drift was different from 0%. In this figure the represented displacements are not the actual out-of-plane
21 displacements measured by the markers, instead they have been post-processed in order to obtain a comparable shape between
22 load stages at which an out-of-plane drift was imposed at the top of the wall and load stages at which no such out-of-plane drift
23 was imposed. This rectification was performed by: (i) fitting a line between the out-of-plane component of the markers at the top
24 beam (no. 239) and foundation (no. 222), at each load stage; (ii) computing the rectified displacement as the difference between
25 the out-of-plane coordinate as measured by the markers along the wall height, and the previous fitted line.

26 The resulting plot indicates that when the top of the wall was displaced towards the East direction, i.e., in the opposite direction
27 to which the wall had developed out-of-plane deformations, the out-of-plane displacements increased further. When it was
28 loaded towards the West direction, the rectified out-of-plane displacements decreased. The trend is clearly visible when loading
29 LS55→LS56 (δ_{ip}=0%), i.e. West→East, during which the maximum out-of-plane displacement at mid-height increased by

1 around 40%. Another interesting observation results when comparing the load stages LS33 and LS43 (δ_{ip}=-0.5%), in which the
2 wall was respectively -0.5% and 0.5% out-of-plane drift; in this case the load stages were not consecutive and since in-between a
3 clover leaf cycle was applied, the out-of-plane displacement not only increased but doubled due to a reduction of the out-of-plane
4 stiffness.

5 The increase of out-of-plane deformations due to the imposed out-of-plane displacements at the top of the wall is the result of the
6 second-order out-of-plane moment, which adds to the pre-existing one (see discussion in Section 5.2) and is illustrated in Fig.
7 14(b).

(a)   (b)
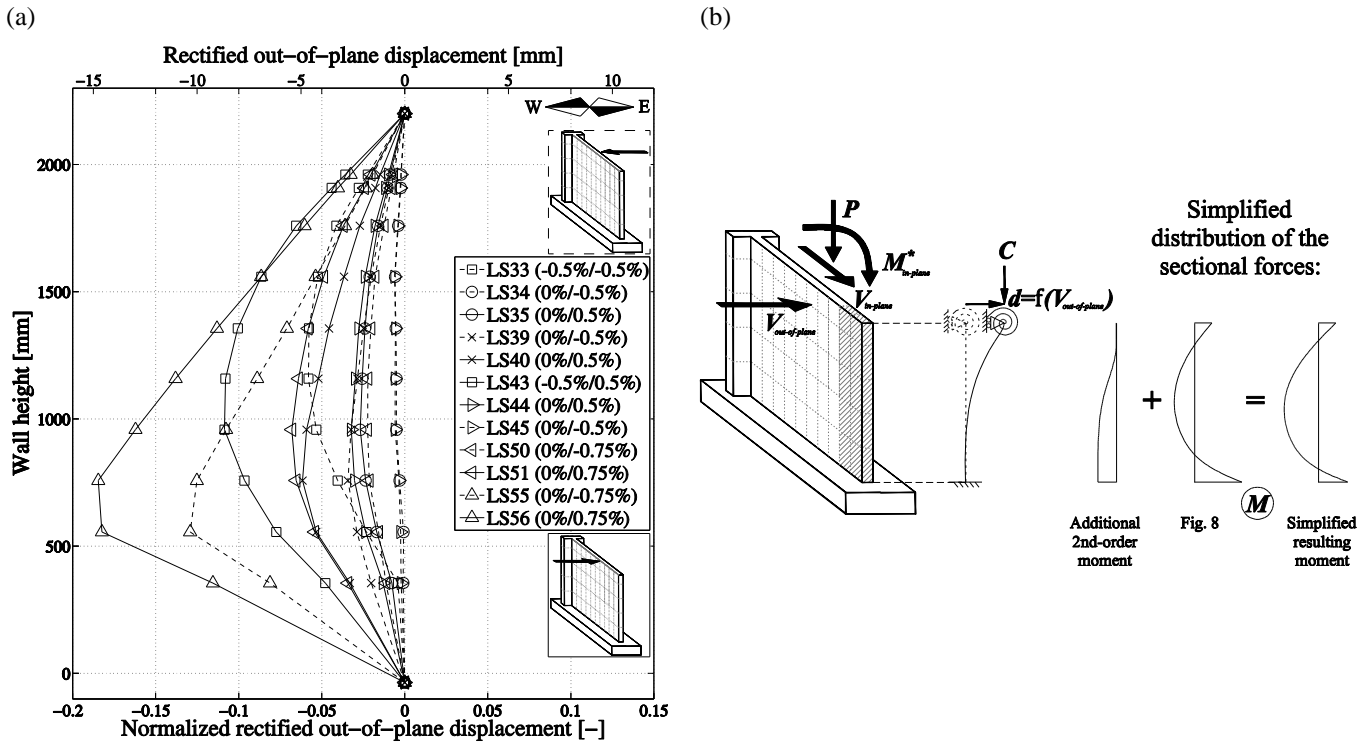
8 **Fig. 14 a** Rectified normalized web edge out-of-plane displacement profile along the wall height at specific load stages for wall
9 TW4, when out-of-plane drift was different from 0% (in-plane/out-of-plane drifts are indicated in parentheses). **b** Equivalent
10 beam model for wall web edge when an out-of-plane displacement is imposed at the top of the wall.

11 *5.3.5   Interaction between the out-of-plane deformations and the out-of-plane forces*

12 As discussed in Section 5.1, the out-of-plane displacements for TW1 at the top of the wall were restrained by four bars and the
13 forces in these bars were estimated from strain gauges. In TW4 the out-of-plane displacements at the top of the wall were
14 controlled by two servo-controlled actuators and the applied forces were measured by load cells in these actuators. Fig. 15
15 depicts for TW1 and TW4 the values of the out-of-plane forces for two cycles at 0.15% and 0.75% in-plane drift; the choice of
16 these two drifts is motivated by the fact that they are representative of the global behaviour before and after the occurrence of
17 significant out-of-plane deformations.

18 The interpretation of the magnitude, direction and evolution of the out-of-plane forces at the top of the wall is a very challenging
19 and complicated task as it depends on a number of factors that interact mutually, namely: wall damage progression, evolution of
20 the out-of-plane instability, influence of minor eccentricities in the placement of both the vertical and the horizontal actuators,
21 small clearance between the hinges of the four bars and the restrained wall (for TW1), imposed out-of-plane bending (for TW4),
22 torsional stiffness of the wall, etc. Therefore, the authors will limit themselves to the following simple observations. The forces
23 required to restrain the out-of-plane displacements at the top of TW1 are in general small, being largest at 0% in-plane drifts
24 when the out-of-plane displacements are largest (e.g., represented as 28→29 in Fig. 15a). In TW4, when passing from negative
25 to positive out-of-plane drifts (from West to East), one could expect an increase in the applied out-of-plane forces. This
26 behaviour is evident when loading from LS16 to LS17 in Fig. 15(b), but when loading from LS50 to LS51 we can observe an
27 opposite trend. This relates to the fact that when pushing towards East (LS16 to LS17) an increase in the out-of-plane

1 displacement was noted, but when pushing towards West (LS 50 to LS51) the out-of-plane displacements decreased, as described
2 in Section 5.3.3. To sum up, the forces required to restrain the out-of-plane displacements at the top of the wall are naturally
3 much smaller than the in-plane forces and will not be relevant when designing the structural system of the building. For walls
4 that are subjected to in-plane displacements only, the out-of-plane forces are largest at 0% in-plane drift, i.e. when the out-of-
5 plane displacements are largest. For walls that are subjected to in-plane and out-of-plane displacements at their top, the trends are
6 less clear as several effects contribute to these forces.
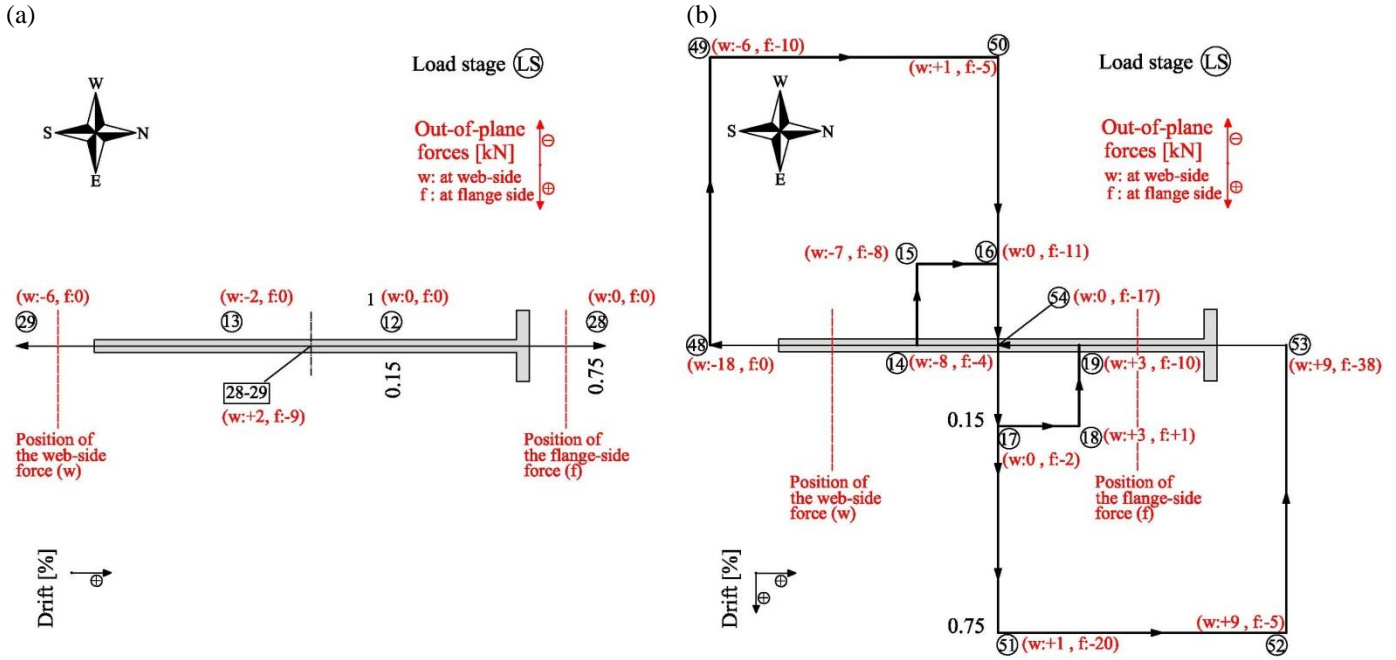
7 **Fig. 15** Identification of the out-of-plane forces at the top beam level, at the web (w) and flange (f) side, in two illustrative cycles
8 (0.15% and 0.75% drift): **a** internal forces in the steel tubes used in TW1 test; **b** forces in the out-of-plane actuators in TW4 test.

9 5.4   Analysis of local-level response quantities

10 *5.4.1   Influence of the tensile strain*

11 As introduced in the initial sections, the maximum tensile strain has been recognized as the critical parameter influencing the
12 lateral stability of walls in literature models. Fig. 16 confirms this finding for the wall tested as it depicts a very clear relation
13 between the maximum out-of-plane displacement and the maximum tensile strain attained at the previous load stage, as
14 computed from the variation of displacements between the LEDs no. 222 and no. 239. The figure also includes a dotted line with
15 the critical value of the tensile strain that triggers wall instability according to the model by Paulay and Priestley (1993), which
16 by application of eq. (3) gives $\varepsilon_{sm,c}$=0.0033 and $\varepsilon_{sm,c}$=0.0036 respectively for walls TW1 and TW4. Again, this value can perhaps
17 be accepted as an indicative value above which considerable out-of-plane displacements are expected, but not as the critical limit
18 to attain failure. Fig. 16 also suggests that the estimation of the maximum out-of-plane displacement, which is lacking in current
19 models, can be related to the maximum tensile strain (possibly combined with additional parameters).

20 *5.4.2   Relation between in-plane drift, out-of-plane deformations and local crack closure*

21 As mentioned in section 5.2, the larger out-of-plane deformations were attained at around 0% in-plane drift when loading from
22 the flange to the web edge, after which a complete recovery of the out-of-plane displacements took place (except in cycle
23 LS30→LS31, where failure was attained). A similar behaviour was also observed in other past experimental tests (Goodsir 1985;
24 Johnson 2010), see Table 1, but never underlined in the reports. This phenomenon is not clearly observable for TW4 in Fig.
25 10(b), except in the last cycle before failure where after attaining the maximum out-of-plane displacement at around 0% in-plane
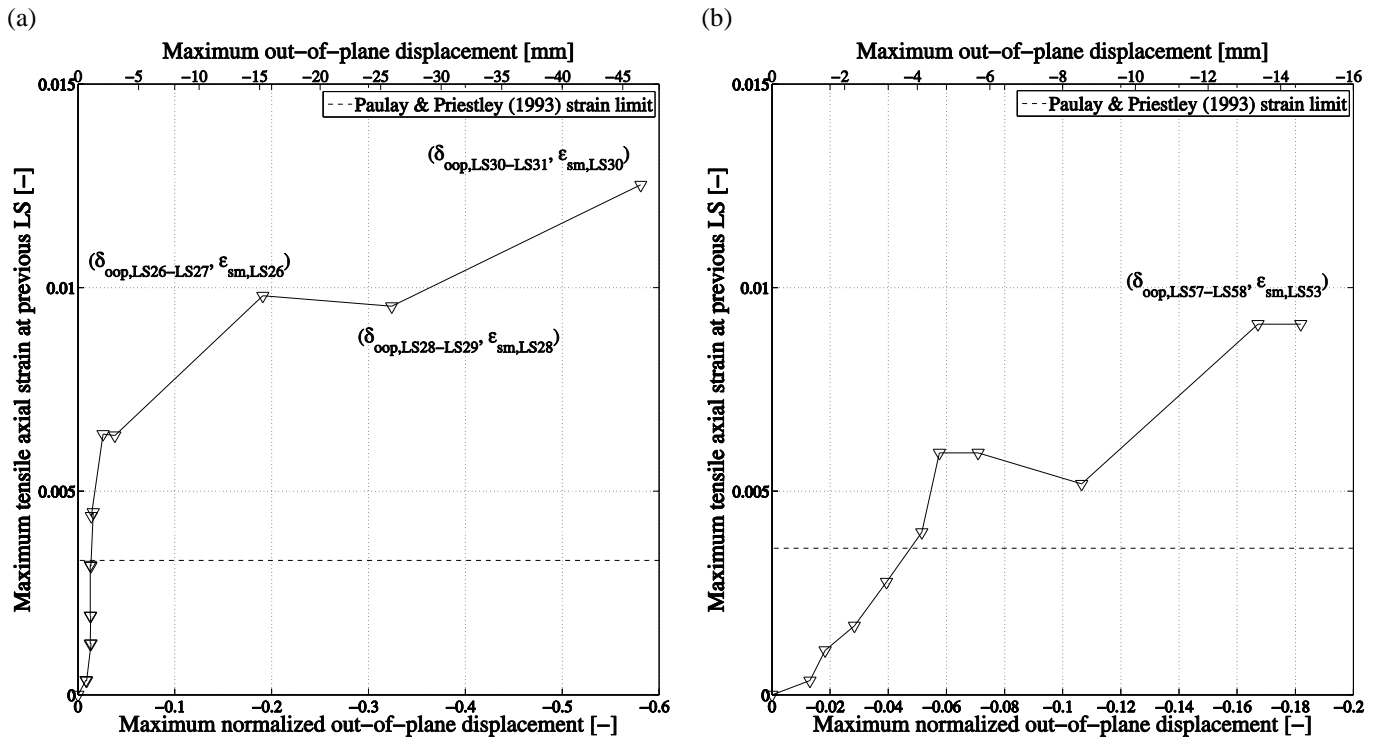26 and 0% out-of-plane drift, a small recovery took place.

27

Fig. 16 Maximum out-of-plane displacement attained between each two consecutive LS *vs* axial tensile strain attained at previous LS with web edge in tension: **a** wall TW1; **b** wall TW4 (only LS at 0% out-of-plane drift are presented in this figure).

In order to understand this effect, it is useful to recall the mechanics of buckling discussed in Section 2.1. One could expect that the straightening up of the wall would only take place once negative (compressive) values of the computed strains are reached (Fig. 11). Focusing on TW1 and noting that the grid of LEDs was placed on the concave side of the wall, it could seem surprising at first that the results of Fig. 11(a) do not back up the previous rationale and that the wall starts to straighten before negative strains are reached (at around $\varepsilon_{sm,c} \cong 0.0015$). The strains shown in Fig. 11 are, however, average strains over the storey height h_w. A similar plot for local axial strains—obtained from the pairs of LEDs no. 2-6, no. 6-8, and no. 8-10, identified in Fig. 4(b)— confirms that the decrease in out-of-plane displacement is indeed linked to the closure of some cracks, i.e., to reaching locally negative (compressive) strains. In particular, Fig. 17(a) shows that for the central pair of LEDs, wherein out-of-plane curvature is maximal, clear compressive strains are reached indicating crack closure.

Simultaneously, the evolution of strains obtained from the pairs of LEDs above and below indicates that the corresponding cracks only close when the out-of-plane deformations reduce considerably, i.e., for larger in-plane displacements (towards negative values of in-plane drift). Fig. 17(b) provides an idea of the extension, along the wall length, of the band at the wall mid-height in which cracks close, contributing to stabilize the wall. Finally, it is noted that upon unloading and reloading in the opposite direction (web to flange, i.e. from odd to even load stages), the out-of-plane displacements remain negligible.

5.4.3   Influence of the crack pattern evolution on the out-of-plane behaviour

Fig. 18 shows the crack patterns of TW1 and TW4 at the same values of drift—0.75% in-plane and 0% out-of-plane— corresponding to load stages LS26 and LS53 respectively. As observable from these photos, even if the patterns seem relatively similar, in TW1 a larger crack at around mid-height can be observed and this difference may have caused the attainment of a larger out-of-plane displacement in this test unit; when starting to load the web edge in compression, in fact, at around 0% in-plane drift the compressive strains concentrated all in this crack (see Fig. 19(a)), causing an increase of the out-of-plane displacement. In TW4, instead, the crack widths were in general smaller (except for a large crack at the base) and more uniformly distributed (see Fig. 19(b)), and this pattern may have favored a faster closure of the cracks, limiting the out-of-plane displacement of the overall wall. It is not possible to say whether the better distribution of crack widths was related to the bi-directional loading or aleatory variability.

The application of uni- or bi-directional loading does not seem to have affected considerably the evolution of the crack pattern, while these may play a relevant role in the development of the out-of-plane instability, as already discussed. The main difference

1 in the crack pattern of the two walls consisted in the crack that developed at the base: the latter in TW4 was larger than in TW1,
2 probably due also to the application of the out-of-plane loading that may have caused an increase of its width.

3 In the test units spalling occurred always only at the base of the wall, where the in-plane moment and therefore also the
4 compression force in the boundary element were largest. Spalling did not seem to have a significant effect on the out-of-plane
5 instability potential, since the lateral displacements were induced mainly by cracks forming clearly above the wall base. This
6 observation may question the influence that spalling can have on the increase of out-of-plane displacements due to a reduced
7 wall thickness and consequent extended susceptibility to tensile strains as it was suggested by the NIST report (NIST 2014). Note
8 that such rationale may not apply to column tests, where the axial load is constant over the height of the column. Therein,
9 spalling will most likely occur at midheight where out-of-plane displacements are largest and might, for this reason, affect the
10 global out-of-plane response.
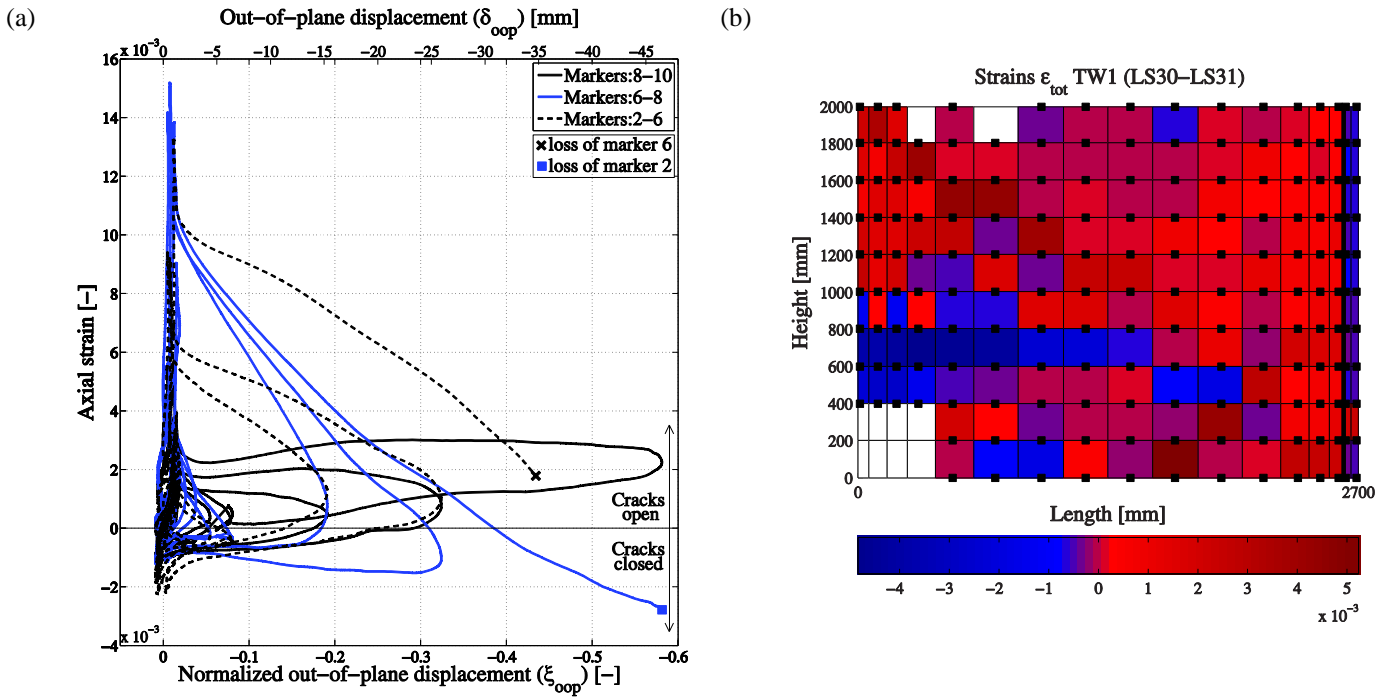
11 **Fig. 17** TW1: **a** Out-of-plane displacement *vs* 'local' axial strain as computed between the indicated pairs of LEDs; **b**
12 Distribution of axial strain throughout the wall when the maximum out-of-plane displacement was attained (during loading
13 LS30→LS31, at ξ_{oop}=0.518).
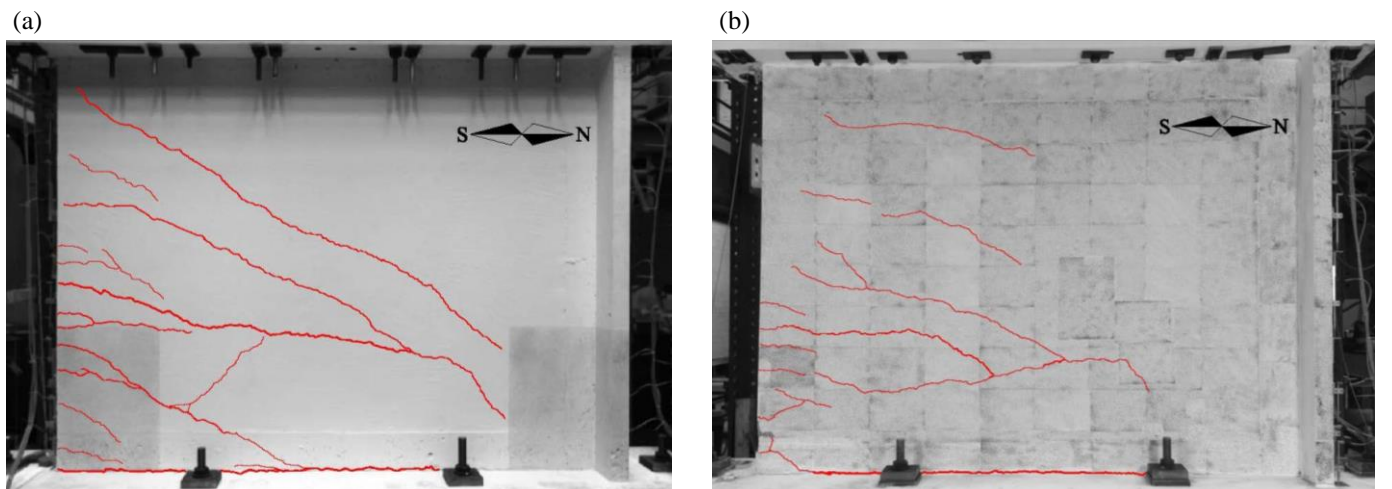
14 **Fig. 18** Crack pattern on the West side of the test units, when they were loaded at 0.75% in-plane and 0% out-of-plane drift: **a**
15 wall TW1 (LS26); **b** wall TW4 (LS53).

22

(a)   (b)
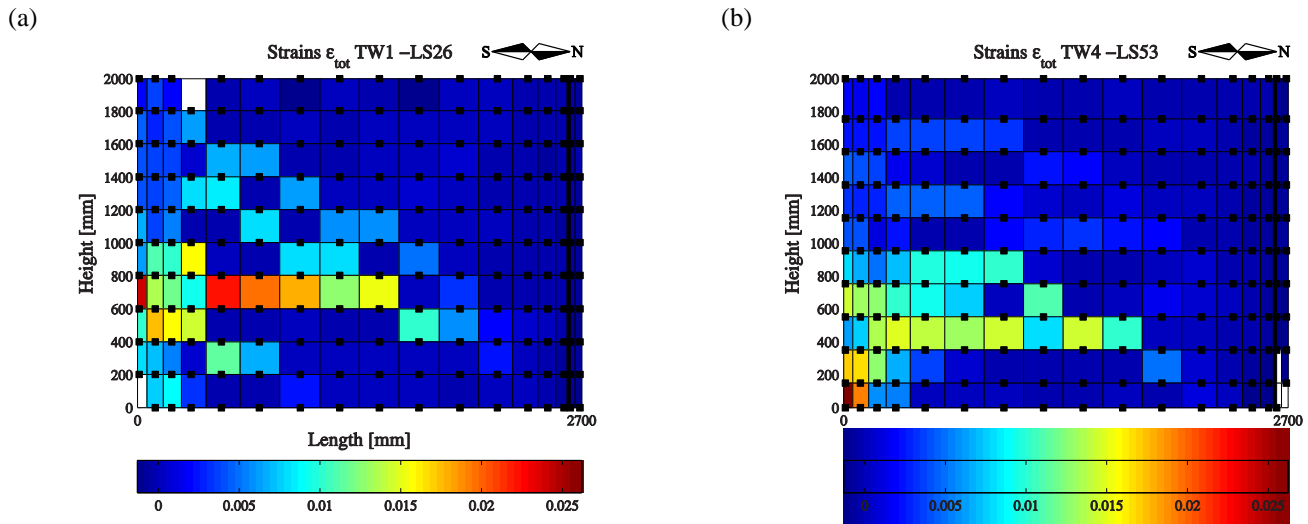
Fig. 19 Distribution of 'local' axial strain (positive values refer to tensile strains) throughout the test units at the first cycle at 0.75% in-plane and 0% out-of-plane drift, when the web edge is in tension: **a** wall TW1 (LS26); **b** wall TW4 (LS53).

6   Conclusions

Following a review on the out-of-plane wall buckling mechanics (Goodsir 1985; Paulay and Priestley 1993), current modelling techniques (Paulay and Priestley 1993; Chai and Elayer 1999; Dashti et al. 2014a), main international code requirements for thin walls (CEN 2004; Standards New Zealand 2006; ACI Committee 318 2011) and past wall test programs where out-of-plane instability was observed (Oesterle et al. 1976; Goodsir 1985; Thomsen and Wallace 1995; Johnson 2010), the present paper describes the results of two experimental tests of thin RC walls subjected to uni-directional (in-plane) and bi-directional (in-plane and out-of-plane) loading, wherein out-of-plane instability influenced the observed failure mode.

The 3D coordinates of 255 optical markers on one wall face were continuously tracked to monitor the evolution of the in-plane and out-of-plane displacement field. This novel data allowed formulating a series of observations, which confirm certain assumptions of the state-of-the-art literature on RC wall stability and question others. The wall tests confirmed the influence of:

(i)   the axial strain: the tests corroborated the critical importance of the maximum tensile strain attained in the previous cycle on the observed out-of-plane displacement (Paulay and Priestley 1993).

(ii)   the crack width: several researchers (Chai and Elayer 1999; Shea et al. 2013) reported a relationship between the crack width and the out-of-plane displacement. The influence of the crack width could explain why wall TW1, which was subjected to uni-directional loading, developed larger out-of-plane displacements than TW4, which was subjected to bi-directional loading. For TW1, one crack at the height where the maximum out-of-plane displacement developed was significantly wider than the others, while for TW4 several cracks developed similar widths.

(iii)   the eccentricity of the longitudinal reinforcement: according to the existing models, until crack closure the compressive force is resisted solely by the rebars and, because of misalignments in the placement of the reinforcement, out-of-plane deformations may be induced (Paulay and Priestley 1993). The result of the tests indicates that the presence of an eccentricity in the placement of the vertical rebars influenced the direction to which the global out-of-plane deformation took place, which can be explained by simple moment equilibrium considerations.

A key observation is that in wall TW1 the largest values of out-of-plane displacement are attained close to 0% in-plane drifts. As stated in Section 4, this observation is not strictly novel (Goodsir 1985; Johnson 2010), but previous researchers did not provide continuous recordings of out-of-plane displacements over full drift cycles. Moreover, the tests showed that taking axially loaded columns that are pinned at both ends as proxies for boundary elements of walls falls short of the reality with regard to:

(i)   the out-of-plane displacement after which failure is expected: considering the test unit which was subjected to in-plane loading only, the wall attained an out-of-plane displacement larger than half the section thickness followed by an almost complete recovery before failure. According to the column models the wall should have failed at a much smaller out-of-

plane displacement. This evidence shows room for improvement of the stability criterion proposed by Paulay and Priestley (1993) and in particular the boundaries conditions of the wall in the out-of-plane direction could be revised.

(ii)   the buckling length: the plastic hinge length does not yield a good approximation of the buckling length, as might be observed also in other tests (Goodsir 1985; Thomsen and Wallace 1995) and numerical simulations (Dashti et al. 2014a). Therefore for future models the previous assumption of $l_0=l_p$ could be revised. The two tests suggested that a larger part of the wall height is involved in the out-of-plane mechanism and the distance between the inflection points was approximately 75% of the storey height.

(iii)   the stabilizing effect of the flange was evident: while the web edge showed large out-of-plane deformations, the web adjoining the flange did not experience relevant out-of-plane displacements.

Finally, it was observed that the imposition of an out-of-plane displacement at the top of the wall increases the global out-of-plane deformations if it is applied in the opposite direction of the latter and decreases if applied in the same direction. Based on these new observations the authors are reviewing the existing phenomenological approaches and developing simple beam finite element models that can be used in engineering practice to assess the out-of-plane instability of wall boundary elements. It is noted that the entire experimental data set is available to the public (Almeida et al. 2015).

Acknowledgments

References

ACI Committee 318 (2011) Building Code Requirements for Structural Concrete (ACI 318M-11) and Commentary. American Concrete Institute, Farmington Hills, U.S.

Almeida JP, Prodan O, Rosso A, Beyer K (2015) Tests on thin reinforced concrete walls subjected to in-plane and out-of-plane cyclic loading (manuscript in preparation). Earthq. Spectra

CEN (2004) Eurocode 8: Design provisions for earthquake resistance of structures - Part 1: General rules, seismic actions and rules for buildings. European Committee for Standardization, Brussels, Belgium

Chai YH, Elayer DT (1999) Lateral stability of reinforced concrete columns under axial reversed cyclic tension and compression. ACI Struct J 96:1–10.

Chrysanidis TA, Tegos IA (2012) The influence of tension strain of wall ends to their resistance against lateral instability for low-reinforced concrete walls. 15th World Conf. Earthq. Eng.

Corley WG, Fiorato AE, Oesterle RG (1981) Structural walls. ACI Spec. Publ.

Creagh A, Acevedo C, Moehle JP, et al (2010) Seismic performance of concrete special boundary element. University of Texas at Austin and University of California Berkley, U.S.

Dashti F, Dhakal RP, Pampanin S (2014a) Simulation of out-of-plane instability in rectangular RC structural walls. Second Eur. Conf. Earthq. Eng. Seismol.

Dashti F, Dhakal RP, Pampanin S (2014b) Numerical simulation of shear wall failure mechanisms. 2014 NZSEE Conf.

1　Elwood KJ (2013) Performance of concrete buildings in the 22 February 2011 Christchurch earthquake and implications for
2　　　Canadian codes. Can J Civ Eng 40:759–776.

3　Goodsir WJ (1985) The design of coupled frame-wall structures for seismic actions. University of Canterbury, Christchurch,
4　　　New Zealand.

5　Johnson B (2010) Anchorage detailing effects on lateral deformation components of RC shear walls. University of Minnesota,
6　　　Minneapolis, U.S.

7　NDI (2009) Optotrak Certus HD, Northern Digital Inc. http://www.ndigital.com/industrial/certushd.php.

8　NIST (2014) Recommendations for Seismic Design of Reinforced Concrete Wall Buildings Based on Studies of the 2010 Maule,
9　　　Chile Earthquake. National Institute of Standards and Technology, U.S. Department of Commerce.

10　NSR-10 (2010) Reglamento Colombiano de Construcción Sismo Resistente - Comisión Asesora Permanente para el Règimen de
11　　　Construcciones Sismo Resistentes. Bogotá D.C., Colombia.

12　Oesterle RG, Fiorato AE, Johal LS, et al (1976) Earthquake resistant structural walls - Tests of isolated walls. Portland Cement
13　　　Association, Skokie, Illinois, U.S.

14　Parra PF, Moehle JP (2014) Lateral Buckling in Reinforced Concrete Walls. Tenth U.S. Natl. Conf. Earthq. Eng.

15　Paulay T, Goodsir WJ (1985) The ductility of structural walls. Bull New Zeal Natl Soc Earthq Eng 18:250–269.

16　Paulay T, Priestley MJN (1992) Seismic design of reinforced concrete and masonry buildings, John Wiley. John Wiley and sons

17　Paulay T, Priestley MJN (1993) Stability of ductile structural walls. ACI Struct J 90:385–392.

18　Rosso A, Almeida JP, Constantin R, et al (2014) Influence of longitudinal reinforcement layouts on RC walls performance.
19　　　Second Eur. Conf. Earthq. Eng. Seismol.

20　Shea M, Wallace JW, Segura C (2013) Seismic performance of thin reinforced concrete shear wall boundaries. University of
21　　　California Los Angeles, U.S.

22　Sritharan S, Beyer K, Henry RS, et al (2014) Understanding poor seismic performance of concrete walls and design implications.
23　　　Earthq Spectra 30:307–334.

24　Standards New Zealand (2006) Concrete Structures Standards, Part 1: The Design of Concrete Structures. Standards Association
25　　　of New Zealand, Wellington, New Zealand.

26　Thomsen JH, Wallace JW (1995) Displacement based design of reinforced concrete structural walls: an experimental
27　　　investigation of walls with rectangular and t-shaped cross-sections. Clarkson University, Postdam, U.S.

28　Timoshenko SP, Gere JM (1961) Theory of Elastic Stability. McGraw-Hill Book Company, Inc., New York and London.

29